Two-step conversion of waste plastic into light olefins and aromatics on metal-free carbon felt catalyst under radiofrequency heating

Cuong Duong-Viet, Lai Truong-Phuoc, Jean-Mario Nhut, Lam Nguyen-Dinh, Christophe Michon, Charlotte Pham, Cuong Pham-Huu

Two-step conversion of waste plastic into light olefins and aromatics on metal-free carbon felt catalyst under radiofrequency heating

Cuong Duong-Viet,[a,b] Lai Truong-Phuoc,[a,b] Jean-Mario Nhut,[a] Lam Nguyen-Dinh,[c] Christophe Michon,[d,] Charlotte Pham,[e,*] Cuong Pham-Huu,[a,*]*

[a]*University of Strasbourg, CNRS, Institute of Chemistry and Processes for Energy, Environment and Health (ICPEES, UMR 7515), ECPM, 25 rue Becquerel, 67087 Strasbourg Cedex 02, France*

[b]*Blackleaf SAS, 210 rue Geiler de Kayserberg, 67400 Illkirch, France*

[c]*Department of Chemical Engineering, The University of Da-Nang – University of Science and Technology, Da-Nang 550000, Viet-Nam*

[d]*University of Strasbourg, CNRS, Laboratoire d'Innovation Moléculaire et Applications (LIMA, UMR 7042) ECPM, 25 rue Becquerel, 67087 Strasbourg Cedex 02, France*

[e]*SICAT SAS, 20 place des Halles, 67000 Strasbourg, France*

Corresponding authors:

christophe.michon@unistra.fr (C. Michon)
charlotte.pham@sicatcatalyst.com (C. Pham)
cuong.pham-huu@unistra.fr (C. Pham-Huu)

Graphical abstract

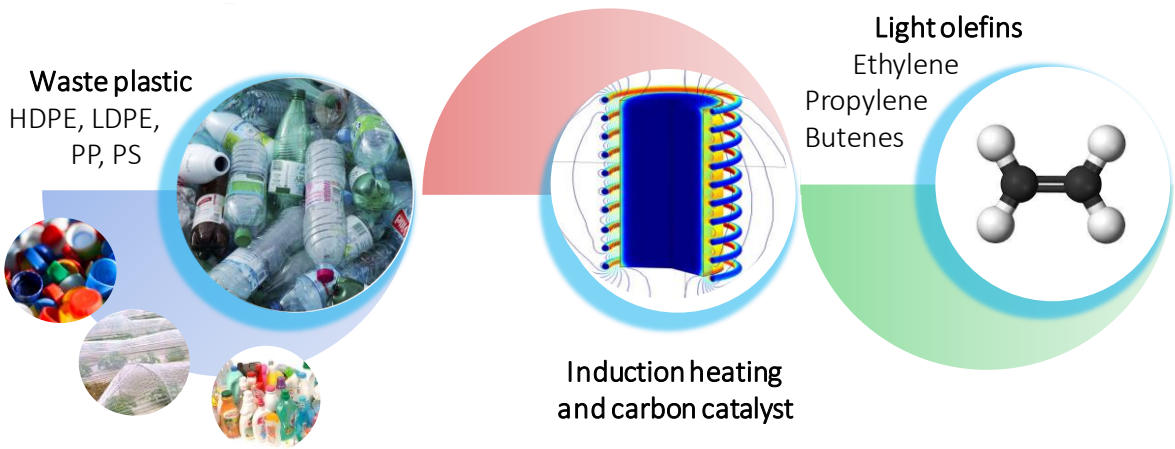

Abstract

Plastic waste represents the most serious global problem for ecosystem and environmental balance, which urges the development of new recycling process for the improvement of circular economy. Chemical recycling of waste plastic to produce back light olefins, ethylene and propylene, is of high interest to reduce the use of fossil sources and allows the direct re-use of waste plastic with a concomitant reduction of associated carbon footprint. In this present work, we report on the development of metal-free carbon catalyst, with high deactivation resistance, coupled with contactless induction heating with high heat efficiency and low energy for the direct conversion of waste plastics back to light olefins and aromatics. Such process is critical yet challenging in industrial applications. Relevant characterizations proved that exclusive surface heating, significantly improves the selective cracking of waste plastics, either model or industrial ones, to produce light olefins and aromatics during long-term operating process. The commercial carbon felt displays remarkable performance for the chemical recycling of waste plastics, surpassing the conventional metal and zeolite catalysts for such relevant environmental problem. The influence of an alternating magnetic field on the catalytic mechanism is advanced to explain such high performance.

Keywords:

Waste plastic – Light olefins – Aromatics – Induction heating – Carbon catalyst – Electrification process

1. Introduction

Plastics represent one of the main commodities for our society in almost every domains spanning from industrial packaging to health care as well as composites for transportation or in different electronic devices. The single-use of plastics, ca. 40%, as commodities represents one of the main sources for the CO_2 release and causes problems for environment and health taken into account that nowadays, about 79% of waste plastic is dumped or landfilled while only a very small amount is recycled (9%) and incinerated (12%) [1, 2, 3]. The landfilling of plastic also contributes to water pollution through waste generated during the extraction and refining of raw materials and from solid waste disposal. The plastic degradation in water leads to the formation of microplastics which can harm marine and human life through transmission within the food chain [4, 5]. New legislations and environmental constraints significantly increase research from both academic and industrial sides to develop new paths for the plastic recycling with the aim to produce value-added products for transportation and petrochemical processes and to reduce the use of fossil resources [6, 7]. Plastic waste as such is contamined with different dopants, which are used for the final packaging depending on the dedicated uses, and thus, preliminary sorting and cleaning are necessary ahead of the recycling process, especially for chemical recycling, as the recycling efficiency and catalyst stability also depend on the nature of the various additives used in the plastic [8]. Nowadays, depending on the quality and purity of the plastic waste, different recycling processes are developed: (*1*) reuse (direct from the plastic waste which can concern a small part of the global plastic produced) [9, 10], (*2*) reprocessing or mechanical recycling with the main concerns due to the gradual decrease of the recycled plastic quality [11, 12], (*3*) depolymerization to produce raw monomeric material (not applicable for all types of plastics), (*4*) thermochemical conversion of the waste plastic into hydrocarbon feedstock [13, 14], and finally, (*5*) energy recovery through incineration with a

concomitant release of CO_2 and some toxic compounds [15, 16]. Among these processes, the thermochemical route allows one to recycle waste plastic fractions that cannot be reused or recycled through mechanical or depolymerization processes and to avoid landfill or incineration. Thermochemical recycling allows one to reduce in a significant manner the greenhouse gas (GHG) emission compared to incineration [17] while remains close, in terms of GHG, to the mechanical recycling as this later can only be applied to a very limited fraction of waste [18]. Recently, several approaches have also been proposed to chemically convert waste polyolefins, especially polyethylene, into valuable products which could be further used as raw materials in several chemical processes [3, 19, 20, 21, 22, 23]. However, the developed processes are mainly relying on low temperature and high hydrogen pressure, which implies challenges for further scaling-up.

Light olefins (ethylene and propylene) represent an important chemical feedstock in chemical industries for the production of polymers, solvents, construction, synthetic fibers, electronic, etc. [24, 25] and are produced in significant volume worldwide and require large amount of fossil compounds. It is estimated that ca. 400 million tons of light olefins (accounted for a total cost of ca. 400 B$ for 2019) are annually produced using billion tons of hydrocarbon feedstock through different processes such as fluid- or steam-cracking or dehydrogenation [26]. Different technologies are used for the production of light olefins from various feedstock such as crude oil, natural gas, coal and biomass, while steam cracking (SC) and fluid catalytic cracking (FCC) represent the main operational processes [27, 28, 29, 30]. The conversion of waste plastic directly into light olefins, C_2-C_4 olefinic fractions, could represent an alternative to the costly depolymerization process, for the supply of light olefins, as monomer subunits to the market, with a concomitant reduction of fossil compounds as raw materials. Thermochemical processes have recently been developed using two-stage process where the first one converts plastic into intermediate hydrocarbons, naphtha fraction, which

are further converted into light olefins through a steam cracker [31, 32, 33]. The light olefins yield amounted between 25 % to 40 % of the inlet hydrocarbons [34, 35, 36]. However, such indirect route remains complex, as the naphtha fraction should be purified to remove all traces of olefins and aromatics, before it could be introduced into the steam cracker and this poses economic and environmental problems. In addition, the residence time should be extremely well controlled as well as steam-to-hydrocarbon ratio to maximize the production of light olefins and to reduce as much as possible undesired secondary reactions [37]. According to the different drawbacks cited before, direct route to convert waste plastic into light olefins, at low to medium temperature and atmospheric pressure (to improve light products yield), with high yield per pass is of high interest. In such thermochemical plastic conversion processes, the acidic zeolites are the most used catalyst in order to perform long-chain polymer cracking to yield liquid hydrocarbon compounds which will be further processed into different high value added fuels such as gasoline, jet fuel or diesel [38, 39, 40, 41, 42]. However, such acidic catalysts are frequently deactivated due to the presence of trace impurities and carbonaceous residue deposit, and thus, requires periodical regeneration, which could have an economic impact on the large-scale development of the process. Meanwhile, a recent study implying iron-based catalyst and microwave has also been reported for the deconstruction of plastic into hydrogen and high-value carbons [43]. Very recently, Conk et al. [44] reported an elegant way to convert high-density polyethylene into propylene, ca. 80 % yield, through a sequence implying dehydrogenation, metathesis and isomerization, using organometallic complexes based on iridium, ruthenium and palladium as catalysts operated under mild reaction conditions. However, despite such promising results, the use of iridium or platinum-based catalysts, noble metals with critical scarcity and high cost, could hamper the future development of the process. In addition, traditional heating via external heater could pose problem of heat transfer, and especially for such high endothermic process. Indeed, the

conductive heating from the reactor periphery induces severe inhomogeneity of temperature inside the catalyst bed, as the heat transfer from outer wall to the center tends to have large thermal resistance due to the long distance of heat conduction through the insulator catalyst layer. Such poor heat transfer leads to a large temperature gradient across the catalyst bed, which is accelerated with the high endothermic character of the reaction.

Recently, it has been reported by different research groups that unusual catalytic processes can be carried out using direct induction heating (IH) in place of traditional heat convection/conduction transfer [45, 46, 47, 48, 49, 50, 51, 52, 53, 54, 55]. In such catalytic process the heat is directly targeted to the solid catalyst without overheating the whole reactor volume and thus, significantly reduce the waste heat associated with the processes [56]. The targeted heat to the catalyst also provides a high efficiency of temperature maintaining to operate catalytic process at kinetic regime by improving the heat transfer and by reducing the problem of heat loss, especially for such high endothermic reaction. In addition, IH also represents a green heating mean for operating catalytic processes as it can be operated using exceeding renewable energy sources (RES), instead of traditional fuel or natural gas burners, for heating up the reactor which thus, contributes to the reduction of the GHG for chemical processes, i.e. electrification of chemical processes [57, 58, 59, 60]. Alongside with magnetic compounds, which can be actively heated by IH, electrical conductors, such as metal or carbon and graphite, could also be efficiently heated up by IH [61, 62]. Recent reports by Pham-Huu and co-workers [63, 64] have pointed out that metal-free carbon catalyst can be efficiently used for the direct catalytic methane decomposition (CMD) to produce turquoise hydrogen under IH mode. The catalyst displays high and stable CMD activity and such catalytic performance was attributed to the fact that the solid carbon deposit plays directly the role of active phase for the CMD process through the formation of vacancies on its surface. Induction heating displays several advantages compared to traditional convection and

conduction heating (CH): (*i*) the heat is directly targeted to the solid catalyst which significantly reduces the heat waste, (*ii*) the temperature maintaining is extremely fast thanks to the instantaneous temperature regulation (several hundred degrees per minute), and (*iii*) the gas-phase is merely heated, mostly through local radiating heat from the solid, and thus, a temperature gradient is created between the solid and gas media which allows the rapid quenching of gas-phase secondary reactions. Finally yet importantly, IH allows one to operate small size plant, which is not possible for conventional heating as for this later, large plant is required for improving the heat production using large gas fuel burners. In the case of IH mode, decentralized plants with on-site and on-demand could be operated with lower environmental impact compared to large ones.

Here, we report on a combination of high heat harvesting carbon-based catalyst and direct IH to crack down a model mixture of polymers (high- and low-density polyethylene (HDPE and LDPE), polypropylene (PP) and polystyrene (PS)) to produce light olefins and aromatics with high yield per pass (ca. 50%) and at medium pyrolysis reaction temperature (atmospheric pressure and $\leq$ 500°C) [65]. Finally, the chemical cracking process was also being experimented on a refusal sorting industrial mixed polymers containing real additives compounds for the complete assessment of the process. The stability of the catalyst was also evaluated through cycling tests using industrial waste polymer. The catalyst was characterized by different techniques and the results are discussed in light of the catalytic performance. The results obtained indicated that the combination of carbon catalyst and contactless IH turns out to be an efficient way to convert waste plastic into light olefins and aromatics with high yield per pass and long-term stability. It is also worthy to note that, by combining carbon catalyst and radiofrequency heating, one can avoid the problem linked with the dependency between the catalyst particle radius and the specific absorption rate, as well as reaction temperature dependency with the Curie temperature of the sample, as usually encountered with magnetic

nanoparticles. In addition, carbon-based catalyst should also display higher deactivation resistance against impurities present in the waste plastic due to its high chemical inertness.

2. Experimental section

2.1 Carbon felt

Commercial filamentous carbon felt (CF), ex-polyacrylonitrile (PAN), with a dimension of 1 × 3 m^2 (thickness of 12 mm) was supplied by Carbone Lorraine (MERSEN, La Défense, France). The as-received CF was cut longitudinally in the form of thin plate (thickness, 3 mm × width, 30 mm), which is further rolled to form a macroscopic cylinder (26 mm x 30 mm) for the experiment. The CF displays a relatively low specific surface area, 4 ± 2 m^2/g measured by means of Kr adsorption, which is mostly linked with its geometric surface area and is in good agreement with the lack of internal porosity of the material (see SEM analysis). The relatively high entanglement of the carbon microfilaments and their high aspect ratio (length-to-diameter ratio) could significantly contribute to the high heat transfer with the induction coil as well as high heat transfer within the catalyst bed through local conduction process.

2.2 Plastic-To-Olefins process

The Plastic-To-Olefins (PTO) process was carried out on a metal-free carbon felt (CF) catalyst in a two stages process. The representative setup used for the process is presented in Fig. 1 with associated legendary for different sections. The first section was consisting in a polymer supplier, which can contain a polymer weight from 10 to 400 g. The reservoir was continuously flushed with an argon flow (30 mL. min^{-1}). The polymer chips (3 mm x 2 mm) were fed to a pre-cracking stage consisting with 4 g of silicon carbide (extrudates with diameter of 3 mm and length up to 4 mm) localized within an electric furnace kept at 450 °C

and continuously flushed with an argon flow with a flow rate of 30 mL. min^{-1}. In the first pre-cracking stage the polymer was decomposed into smaller fragments, i.e. random cracking, to yield both gaseous and liquid compound, which further passed through the connection pipe (100 mm length), maintained at 250°C, into the second cracking stage operated either under direct IH or indirect Joule heating. The outgoing products, from the first pre-cracking stage, were also analyzed through direct cooling in order to get more insight about their nature. At room temperature, the products are in the form of waxy compounds which are hardly solubilized in petroleum ether solvent; this indicates that the pre-cracking stage only crack down the pristine polymer into some long-chain fragments (mostly waxes at room temperature) which will be further cracked into liquid and gaseous hydrocarbons in the second cracking stage.

The second cracking stage is heated up either under direct IH or indirect CH mode. The IH experiment was conducted on an EasyHeat® 8310 induction heating setup (10 kW, Ambrell Ltd) equipped with a spiral 6-turn induction coil (L = 1.05 m, pure coil resistance = $2.066 \times 10^{-3}\,\Omega$) and external cooling chiller with recirculated water/glycerol (10%) mixture as cooling media. In a typical experiment, a quartz reactor ($\varnothing_{inner}$, 24 mm, length, 1,000 mm) containing the catalyst, similar to that used for the CH, was placed inside the induction heater coils (see inset in Fig. 1). The real-time temperature control/regulation was ensured by a PID system (Proportional Integral Derivative controller, Eurotherm model 3504), connected to a laser pyrometer (Optris®, power < 1 mW, located at ≈ 30 cm from the catalyst), focused on the middle of catalyst bed on the external wall of the quartz reactor, and another for the monitoring of the entrance temperature and operates in the range of 150 °C to 1400 °C. The accuracy of the temperature measurement is also monitored using a volumetric thermal camera (Optris, Model PI 1M) operated in a temperature range of 450 °C to 1,400 °C. The heating rate of the system is about 2000 °C min^{-1} in the 160 - 600 °C temperature range which

could allow the efficient temperature maintaining during the highly endothermic cracking process. It is worthy to note that the inductor operated at a frequency of 263 kHz which generated a much lower magnetic field compared to those operated at lower frequency, *i.e.*, < 10 kHz. In order to reduce the exposure of the worker to the magnetic field the setup was localized inside a Faraday cage surrounded with metal mesh.

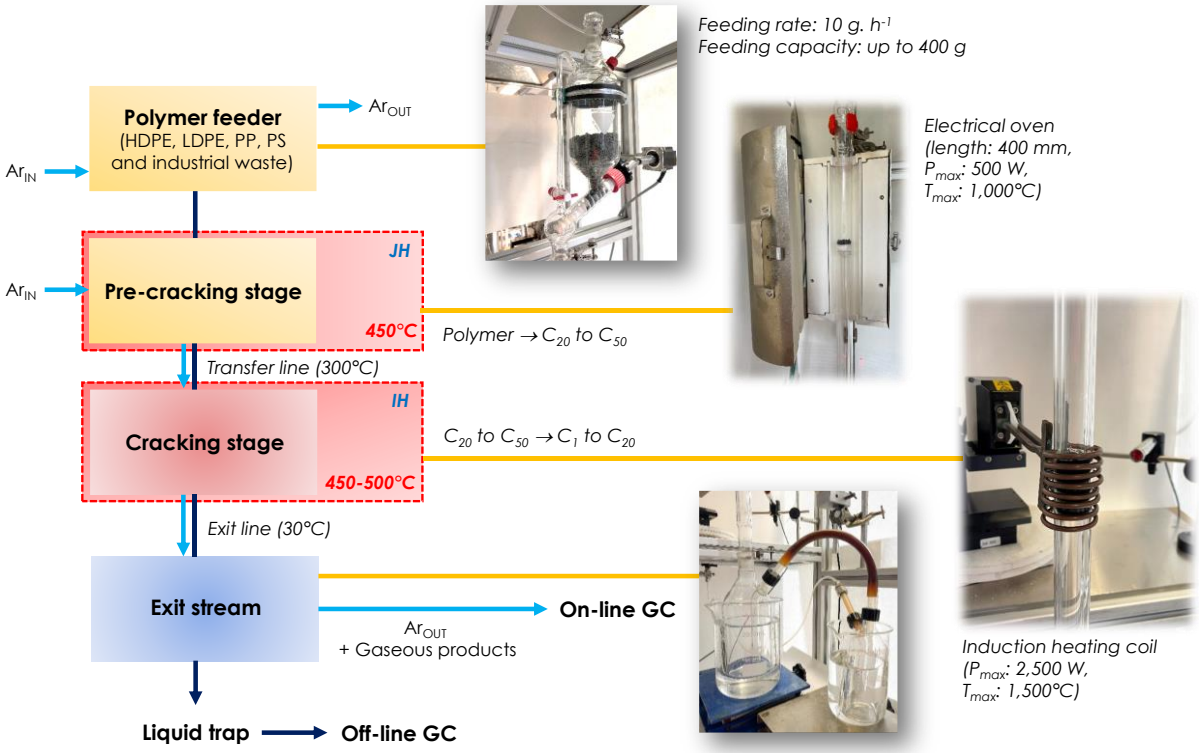

Fig. 1 | Schematic representation of the pyrolysis setup operated under IH mode for converting waste plastic into light olefins and aromatics on CF catalyst. Digital photos of the different sections are also presented.

2.3 Characterization techniques

The scanning electron microscopy (SEM) was carried out on a ZEISS 2600F with a resolution of 5 nm. The sample was deposited onto a double face graphite tape in order to avoid charging effect during the analysis.

The specific surface areas of the catalysts, were determined in a Micromeritics sorptometer. The sample was outgassed at 250 °C under vacuum for 8 h in order to desorb moisture and adsorbed species on its surface. Physisorption measurements were carried out using N_2 as adsorbent at -196 °C under a relative pressure between 0.06 and 0.99. The pore size distribution was calculated from the desorption branch of the isotherm.

Computed X-ray tomography (CT) was performed on an X-Ray Solution tomograph, model Easytom 150–160 (RX solution SAS, Chavanod, France) on the ICS tomography platform (UPR 22, CNRS, Strasbourg, France). The X-ray generator is an open-tube Hamatsu microfocus with tungsten filament and tungsten target. The detector is a Varian PaxScan 2520DX1920x1536 pixel flat panel sensor (pixel size 1/4.127 µ m x 127 µm) – 16 bits. The scan is carried out with the following parameters: Resolution = 1.2 µ m, Source – sampling distance = 3.29 mm, Source – sensor 1/4,347 mm, X-ray energy = 80 kV, beam intensity = 65 µ A. The 1984 projections are made on 360°. Average = 15 images per position. The sensor has a frame rate of 2 frames per second. The entire scan lasts 4.5 hours. The reconstruction method used is filtered rear-projection.

The Raman spectra were recorded using LabRAM ARAMIS Horiba Raman spectrometer equipment. Spectra were recorded over the range of 500 - 4000 cm^{-1} at the laser excitation wavelength of 532 nm. The sample was deposited on glass substrate by deep-coating of its suspension and carefully dried before measurement.

Thermal gravimetric analysis (TGA) was realized on a TGA Q5000 instrument with a heating rate of 10 °C/min under air atmosphere. The weight of the sample was kept at around 10 mg in order to avoid diffusion problems during the analysis.

3. Results and discussion

3.1 Carbon felt characteristics

The characteristics of the carbon felt (CF) used as metal-free catalyst are presented in Fig. 2. For the tests, the rolled CF in a cylinder shape with following dimension: height, 30 mm, diameter, 24 mm and displays an apparent volume of 64 cm^3 is used (Fig. 2a). The CF cylinder displays a large pores connection as evidenced by CT analysis in Fig. 2b and c, which can measure the whole volume of the cylinder with a relatively high accuracy. SEM micrographs with different magnifications reveal the high entanglement of the carbon microfilaments within the sample and the smooth microfilament surface (Fig. 2d to f). High-resolution SEM micrograph in Fig. 2f clearly evidences the non-porous structure of the CF catalyst with a complete lack of internal porosity within the carbon microfilament (indicated by arrow). On such non-porous carbon catalyst, it is expected that the pyrolysis reaction takes place exclusively via external surface without any diffusional phenomenon as generally encountered with zeolite catalysts where pores plugging by solid residue is the main cause of catalyst deactivation alongside with chemical poisoning. The connected voids allow the easy circulation of gaseous or even liquid reactants throughout the CF matrix, which could contribute to high pyrolysis efficiency. The catalytic activity of the CF, containing defects, has already been reported to be an efficient metal-free catalyst for selective oxidation of H_2S into elemental sulfur and confirm it advantage over traditional metal-based catalysts [66].

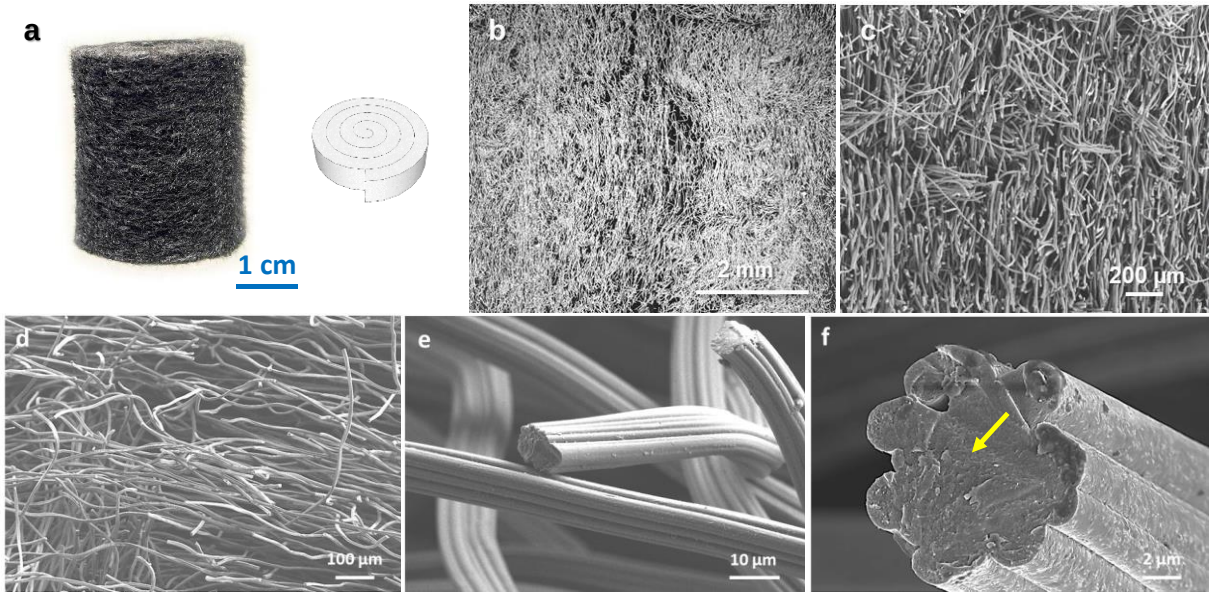

Fig. 2 | (a) Digital photo and drawing of the rolled carbon felt used as metal-free catalyst in the conversion of waste plastic-to-olefins process. (b) CT micrograph and (c, d) SEM images of the rolled CF catalyst showing the entanglement of the carbon microfilament arrangement inside the sample. (e, f) Medium and high-resolution SEM micrographs showing the presence of large voidage within the sample and the smooth surface without internal porosity (indicated by arrows in 2f) in good agreement with the low SSA measured by N_2 adsorption.

The nature of the carbon in the CF sample is investigate by Raman spectroscopy and the results are presented in Fig. 3a. Raman spectra show classical typical D and G bands at 1343 cm^{-1} and 1597 cm^{-1}, respectively. A third band located at 2700 cm^{-1}, noted 2D, is also observed in the Raman spectra which is attributed to the presence of graphene and/or graphene multi-sheets [67]. G band was assigned to symmetric and crystalline sp^2 carbon, while D band was associated with the defects/edges in the in-plane of graphene layers and irregular graphitic lattice on the surface. The I_D/I_G ratio is relatively high at 1.28 and indicates that the sample displays a relatively large number of defects or low graphitization degree. Indeed, the fact that D peak is relatively high could be attributed to the presence of disorder in the graphite plane over long distance. A prominent 2D peak seems to indicate that some surface graphene planes are present in the CF sample, and this could be originated from the production technique. The TGA spectra of the fresh and spent CF catalysts are presented in

Fig. 3b. The CF sample displays a combustion peak at ca. 740 °C, which represents a medium oxidative resistance and is in good agreement with the relatively high graphitization of the CF and also with the Raman analysis presented above. Ammonia titration has evidenced the complete lack of any residual acidic sites on the CF catalyst (not reported) which rules out any influence of such acid sites on the pyrolysis process.

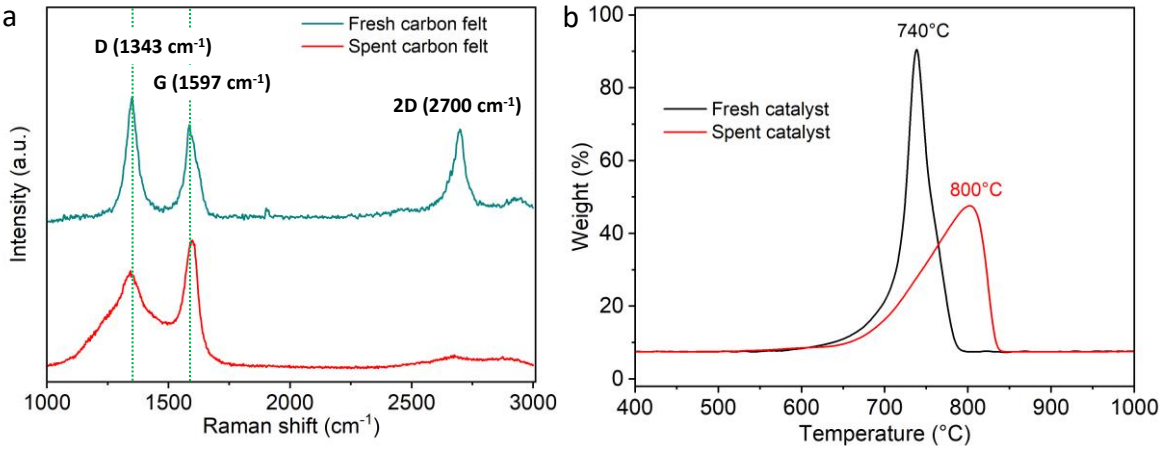

Fig. 3 | (a) Raman spectra of the CF sample, before and after PTO test, at reaction temperature of 500 °C. (b) Corresponding TGA spectra of the fresh and spent catalysts under air (10 mL. min^{-1}).

3.2 Model HDPE pyrolysis

The cracking results obtained on the CF rolled disk at different temperatures are presented in Fig. 4a to c. The CF catalyst displays a maximum cracking performance and light olefins yield at reaction temperature of 450 °C, as at lower temperature liquid hydrocarbon is predominant with lower light olefins fraction (not shown). At reaction temperature higher than 500 °C, extensive cracking yields mostly methane leading to a net decrease of the light olefins yield, and also to the increase of the solid residue deposited on the CF catalyst. Aromatic compounds are also obtained among the reaction products, and are mostly constituted by benzene and toluene: 6 % at 450 °C and 9 % at 500 °C, respectively (Fig. 4c and d). However, it is worthy to mention that the objective of the present process is devoted to

the production of light olefins back from waste plastic and not aromatic compounds according to the relatively low operational temperature. However, the formation of some aromatic compounds could be useful as there are belonging to the five most demanded chemical building blocks for the petrochemical field. Work is ongoing to check out the reaction conditions in order to tune the selectivity of either light olefins or aromatics in the process. The total light olefins and aromatics yield at 450 °C is amounted to about 49 wt. % which represents a highest yield for a one-step pyrolysis process to convert waste plastic into its corresponding monomers and aromatics. Indeed, for a two-stage process, i.e. waste plastic conversion into naphtha followed by steam cracking to produce olefins, the overall olefins yield remains low despite the complexity and high severity of the process, i.e. ≤ 40 % [68, 69].

The reaction seems to occur by adsorption of the intermediate long-chain hydrocarbon pyrolyzed compounds, issued from the first pre-cracking stage, on the external surface of the non-porous CF catalyst followed by a cracking to yield light olefins and aromatics, which could be rapidly desorbed into the gas-phase. Therefore, the reaction would thus proceed in a different way than the traditional ones reported on zeolite and zeolite-based catalysts [70, 71] where light products are mostly formed inside the catalyst porosity after surface cracking to yield smaller fraction which subsequently diffuse inside. In general, on a non-porous material and in the absence of metallic catalyst, long-chain hydrocarbons fraction is generated through external cracking on the surface site of catalysts [72]. As IH only targets heat to the solid and thus, favors the cracking of adsorbed species, the gas phase medium is expected to have a lower temperature allowing a rapid quench of the desorbed light olefins and thus, reducing the secondary gas-phase reactions in a similar way as reported for microwave heating [73, 74]. Similar observation has also been reported by Luo et al. [45] during the catalytic decomposition of medical waste plastic under IH to produce hydrogen-rich gas. The

surrounding magnetic and electric fields, even weak, could also have some influence on the radical production, or reaction intermediate adsorption/desorption, as recently reported from different research groups [75]. Indeed, Essyed et al. [75] have suggested that the presence of both electric and magnetic fields could be at the origin of the ordered graphene-like carbon generated during the catalytic methane decomposition (CMD) process on carbon catalyst and that IH not only provides heat to the catalyst but also intervene itself in the reaction mechanism by modifying the reaction intermediate species.

^{1}H-NMR spectrum presented in Fig. 4d shows the presence of some aromatic compounds inside the liquid medium. Such results have also been confirmed by liquid-phase GC analysis which indicates the presence of aromatics (see discussion below). The NMR analysis of the liquid fraction also indicates that branched alkanes and alkenes are also detected in trace amounts, which is in good agreement with the lack of acidity in the catalyst. Alkenes appeared to be a mixture of terminal and internal aliphatic derivatives with lower amount of aromatic, and could be explained by the random scission mechanism of polyethylene thermal degradation followed by internal rearrangement through radical migration within the hydrocarbon chain. Saturated hydrocarbons are generated by incorporation of hydrogen into the hydrocarbon backbone followed by desorption. Aromatic compounds are also detected in both gaseous and liquid products. According to the fact that the CF catalyst contains no acidic sites, it is expected that these aromatic compounds, detected in the present study, could be issued from the surface reaction between the intermediate olefin species, adsorbed on the carbon surface, and not from the gas-phase condensation process as discussed above. Indeed, Santamaria and co-workers [76] have reported that, during the methane dehydroaromatization (MDA) process operated under microwave heating, where the gas-solid temperature gradient significantly decreases the quantity of aromatic compounds in the exit stream with a concomitant improvement of the amount of primary intermediate

product, i.e. C_2H_2. Such a control of the temperature gradient should significantly decrease the formation of polyaromatic hydrocarbon (PAH) which is a coke precursor and is in good agreement with the results observed in this study where mostly monoaromatics are obtained. The GC results indicate the presence of mostly benzene, toluene and xylene present in the gas phase in the following proportion: ∑BTX = 6 wt. % at 450 °C and ∑BTX = 9 wt. % at 500 °C. The lack of heavier aromatic compounds, polyaromatic hydrocarbons (PAHs) which should be steadily solidify at the exit stream (due to their high liquefaction point), seems to confirm that gas-phase condensation is unlikely to occur due to the specific heat targeting to the solid under IH mode. The aromatic compounds detected by NMR are amounted to ca. 19 % of the total carbon in the liquid fraction and could be attributed to the specificity of IH to heat up surface material. It is worthy to note that the unsaturated hydrocarbons and aromatics which are coke precursors compounds could reacted each other on the catalyst surface upon re-adsorption to produce carbonaceous residues. However, the contribution of such secondary pathway seems to be relatively low at reaction temperature of 450 °C, i.e. 1 wt. % of solid (and some waxy) residue, while it significantly increases at higher reaction temperature, i.e. 9 wt. % at 500 °C (Fig. 4a and b). Such relatively low solid residue could be attributed to the lower re-adsorption rate of the intermediate species due to exclusive surface heating provided by the IH. The high surface temperature could prevent re-adsorption of unsaturated hydrocarbons and aromatics which are coke precursors [77] as adsorption is exothermic process and thus, an increase in surface temperature leads to a decrease in adsorption. Such reaction could be attributed to the presence of eddy thermal effect on the surface of the CF which provided high local temperature compared to a simple thermal-diffusion process [78]. This property has also been used in the field of water splitting in order to achieve the reaction close equilibrium voltage at room temperature whereas it cannot be reached in traditional heating process [79, 80]. The results clearly demonstrate that model HDPE waste plastic can

be efficiently cracked-down into light olefins and aromatics, with a relatively high yield up to 49 %, at moderate reaction temperature, i.e. 450 °C, compared to cracking process of naphtha in traditional steam cracker where reaction temperature is around 1,000 °C [81].

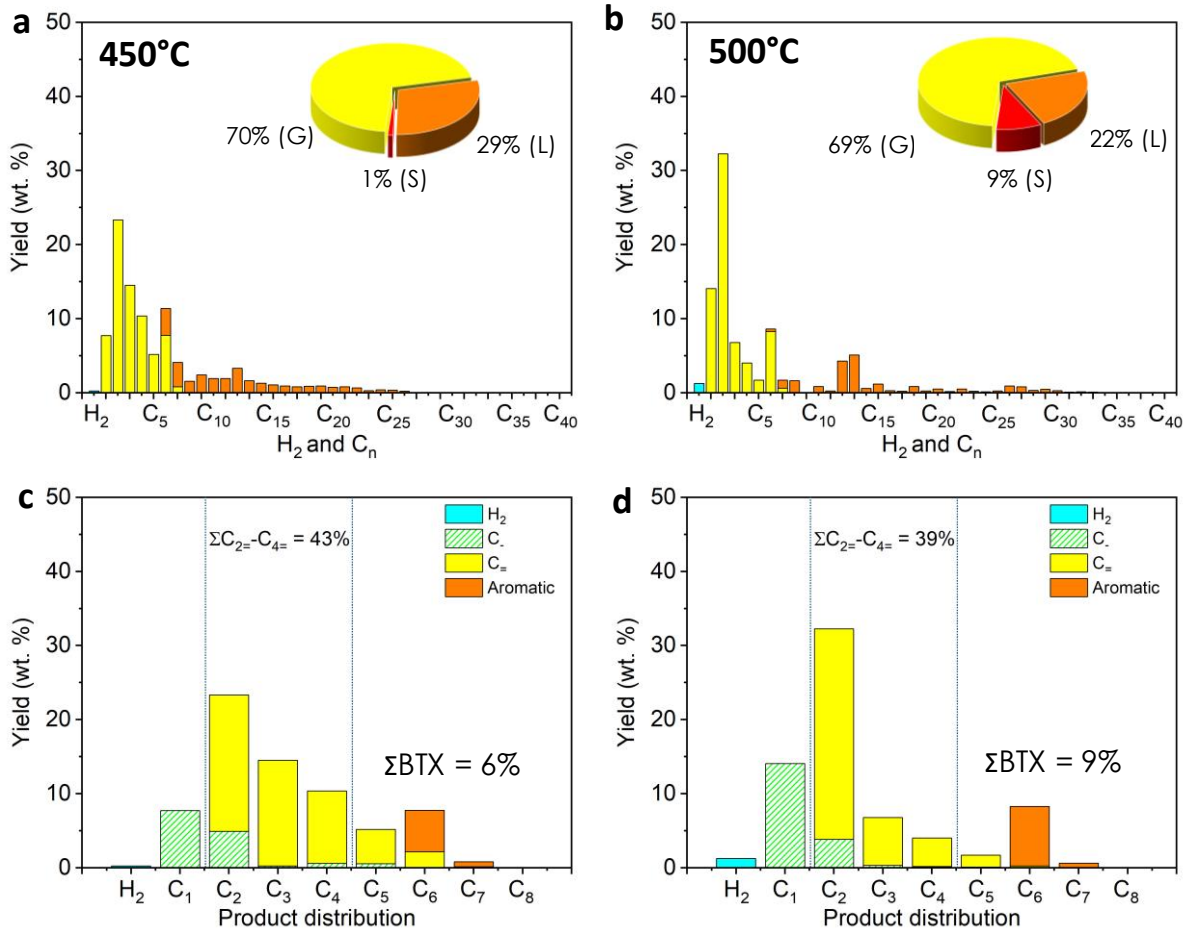

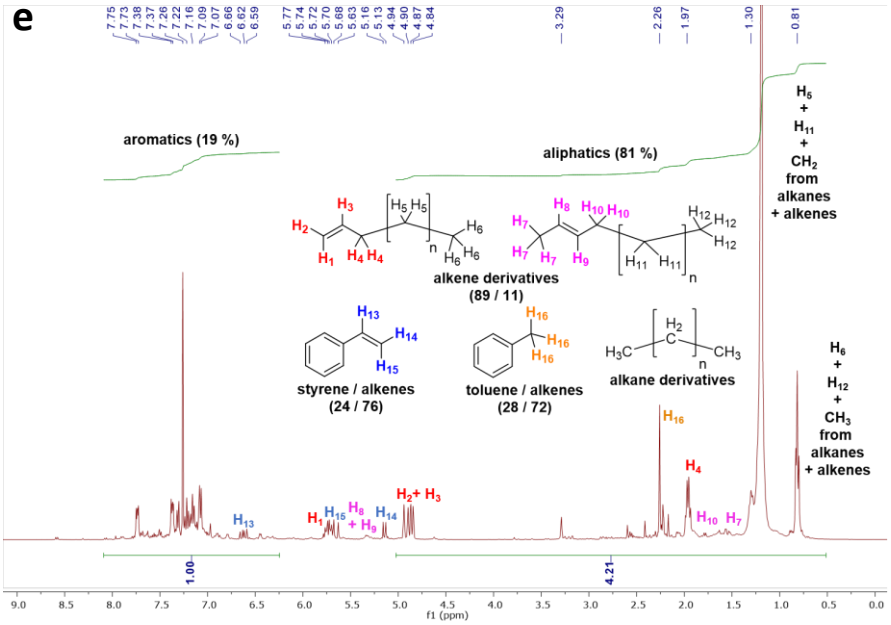

Fig. 4 | (a, b) PTO performance at different reaction temperature using model HDPE on CF catalyst operated under contactless IH in a two-stage reactor configuration. Reaction conditions: polymer weight feeding = 10 g. h^{-1} with sequential feeder, CF weight = 1.6 g (with an apparent volume of 64 cm^3), reactor diameter = 26 mm, argon flow rate (downward) = 30 mL. min^{-1}, reaction temperature = 450°C, and 500 °C, the HDPE was vaporized in a first stage of the process using an electric oven set at 450 °C. (c, d) The light olefins and aromatics hydrocarbons in the gaseous fraction obtained in the different experiments. (e) ^{1}H-NMR spectrum of the liquid phase hydrocarbons condensed at the exit stream of the process.

The same CF catalyst was also evaluated under indirect CH in an electric oven and the results are presented in Fig. 5a and b. Under CH mode most of the waste plastic was converted into liquid and waxy hydrocarbons, which can be partly dissolved in dioxane. The dissolved hydrocarbons fraction contains medium to short chain hydrocarbons ranged from C_{10} to C_{30}. The higher waxy hydrocarbons which was not dissolved in dioxane, $C_nH_{2n+2} > C_{30}$, cannot be analyzed. Such results definitively confirm the high efficiency of IH to operate PTO process compared to conventional CH as already reported from several studies in the literature.

The high PTO efficiency observed on the CF material under IH, unlikely to that obtained under CH, could be attributed to the following facts (the influence of the magnetic field will be discussed apart below): (*i*) high temperature maintaining efficiency due to the

high heating rate of the IH, i.e. several hundred degrees per minute, to maintain the material temperature at the set value for the endothermic cracking reaction; and, (*ii*) better temperature homogeneity within the entire solid bed as the heat is generated directly within the material body and not through convection/conduction indirect transfer as encountered with the indirect CH mode. Indeed, carbon felt is well known as insulator shield material to prevent heat transfer for high temperature oven, and thus, the carbon filaments display high heat transfer along its filamentous structure but not between the filaments due to the presence of large voidage in the material. In the case of IH, the entire solid volume can be heated while in the case of CH the heat is transferred along the external filaments to the core of the solid bed, which is more affected by the filamentous structure with large voidage of the material. Such heat resistance can be avoided with IH as heat is directly generated through the material body as discussed above and the heat distribution throughout the carbon microfilaments is much faster due to their small diameter, which remains within the range of depth penetration for the eddy currents, i.e. few micrometers from the outer surface. The high aspect ratio (length vs diameter) of the carbon microfilaments constituting the CF material also contributes to rapid heat conduction along the filaments and through the entire material matrix and thus, greatly improve the reaction process. The high heat maintaining, especially on the catalyst surface where the chemical process takes place, is of high interest as it allows the direct and rapid temperature compensation due to the highly endothermic reaction. Zhang et al. [82] have reported the conversion of waste plastic on acidic carbon-based catalysts operated at relatively high reaction temperature, i.e. 600°C, to produce jet fuel liquid hydrocarbons. According to such results the direct conversion of waste plastic into gaseous light olefins is unlikely to occur at reaction temperature ≤ 600°C. Similar results between IH and CH modes have also been reported during the plastic-to-fuel process operated on a medium SSA mesoporous carbon (300 m^2. g^{-1}) under both IH and CH modes [83]. In such report at the same reaction

temperature the porous carbon mostly yields liquid hydrocarbons from the pyrolysis of waste plastic while in the present work, non-porous microfilaments mostly yield light olefins and gaseous hydrocarbons. Such results could be explained by the presence of a large porosity network in the mesoporous carbon which allows rapid intermediate hydrocarbons diffusion inside the catalyst matrix where cracking is initiated. Plastic cracking is a highly endothermic reaction and thus, the products formation could be strongly linked to the catalyst temperature. In the case of mesoporous carbon, it is suggested that some temperature gradient could exist between the carbon surface (thin layer of heating by skin effect) and its core, which could reduce the efficiency of the cracking leading mostly to medium chain hydrocarbons. The small diameter of the CF microfilament (10 µm) also significantly contributes to a high heat transfer and maintaining compared to that of the mesoporous carbon with larger diameter (3 mm). Such an effect of the surface temperature could also be advanced to explain the formation of a relatively large amount of aromatic compounds, i.e. 19 % vs 1 %, in the liquid fraction of the CF vs mesoporous carbon catalyst. One cannot exclude the different interaction between the carbon catalyst and the magnetic field which could led to a different reaction mechanism between the two carbon catalysts (see discussion below).

In addition, as stated above the presence of a surrounding magnetic field, even small at ca. 20 mT, could also have an influence on the adsorption and cracking process. Kiatphuengporn et al. [84] reported about 50 % increase in the rate of CO_2 hydrogenation on a Fe/MCM-41 catalyst operated under an external magnetic field of 30 mT alongside with a decrease of about 20 % of the activation energy. The influence of magnetic field on the physisorption and chemisorption of reactant gases on the magnetic catalyst has been advanced by the authors to explain the observed results. The cracking of plastic intermediates could give rise to radical species through the breaking of C-C bonds with lower strength than the C-H bonds, as reported in a review by Gholami et al. [68], which could be influenced by the

magnetic field according to the reports by Liu et al. [85] and by Harmon et al. [86]. Liu et al. [84] and Ikeya et al. [87] have stated in their reports that magnetic field could stabilize radical species leading to an off-equilibrium chemical process. Rodgers [88] has also reported that the exchange between the singlet and triplet states under an external magnetic field could led to a so-called radical pair mechanism in chemical process. The presence of adatom (carbon) or defects (vacancies) also induce magnetic character sites on the carbon material which could participate in the adsorption of the radical intermediates and allow the reaction to proceed forward [89, 90, 91]. Recently, Adogwa et al. [92] have advanced an interesting hypothesis about the role of alternative magnetic field on the adsorption and desorption of the reactant on the catalyst surface to explain the high catalytic performance of CO oxidation, almost an order of magnitude, on the Pt/Fe_3O_4 catalyst operated under IH mode. The authors have observed that infrared (IR) peaks corresponding to *CO-Pt at 2063 cm^{-1}, gaseous CO at 2118 and 2171 cm^{-1}, and a negligible gaseous CO_2 (2400 and 2300 cm^{-1}) were rapidly changed to a prominent formation of gaseous CO_2 upon introducing an oscillating magnetic field of 24 mT (which is very similar to that the field used in the present work). Such results confirm the high influence of the oscillating magnetic field to facilitate *CO oxidation. The same IR peaks are restored after removing the magnetic field for about 60 s. The observed results were attributed by the authors to the presence of an oscillating magnetic field which could improve on one side, the adsorption state of the reactant, and on the other, the combined desorption of the product. The oscillating magnetic field could modify the binding energies of surface intermediates, eg. A* and B*, over a broad range of frequencies. Such oscillating frequency could allow the most abundant B* formation from A* → B* before switching to favor B* → B + *, and thus, breaking the Sabatier limit, which stated that the reaction intermediates should avoid binding to the catalyst surface either too weakly or too strongly to achieve high activity. Such hypothesis remains very similar to that reported before by Kiatphuengporn et

al. to explain the possible influence of a magnetic field on the catalytic performances [83]. Recent results reported by Essyed et al. [74] during the catalytic methane decomposition (CMD) process on carbon-based catalyst operated under IH also pointed the same positive influence of an oscillating magnetic field on the catalytic performance. The authors have observed that carbon-based catalyst under IH displayed a relatively high methane conversion up to 60 % whereas the same catalyst, operated under traditional convection and conduction mode without an external magnetic field, only displayed about 2 % of methane conversion. Magnetic field allowing the stabilization of intermediates radical species was advanced by the authors to explain the observed results. These latest results pointed out that IH not only improve heat transfer to the catalytic system but also actively participate in the reaction pathway itself, by modifying either the adsorption and conversion rate of the intermediate species or the reaction mechanism itself.

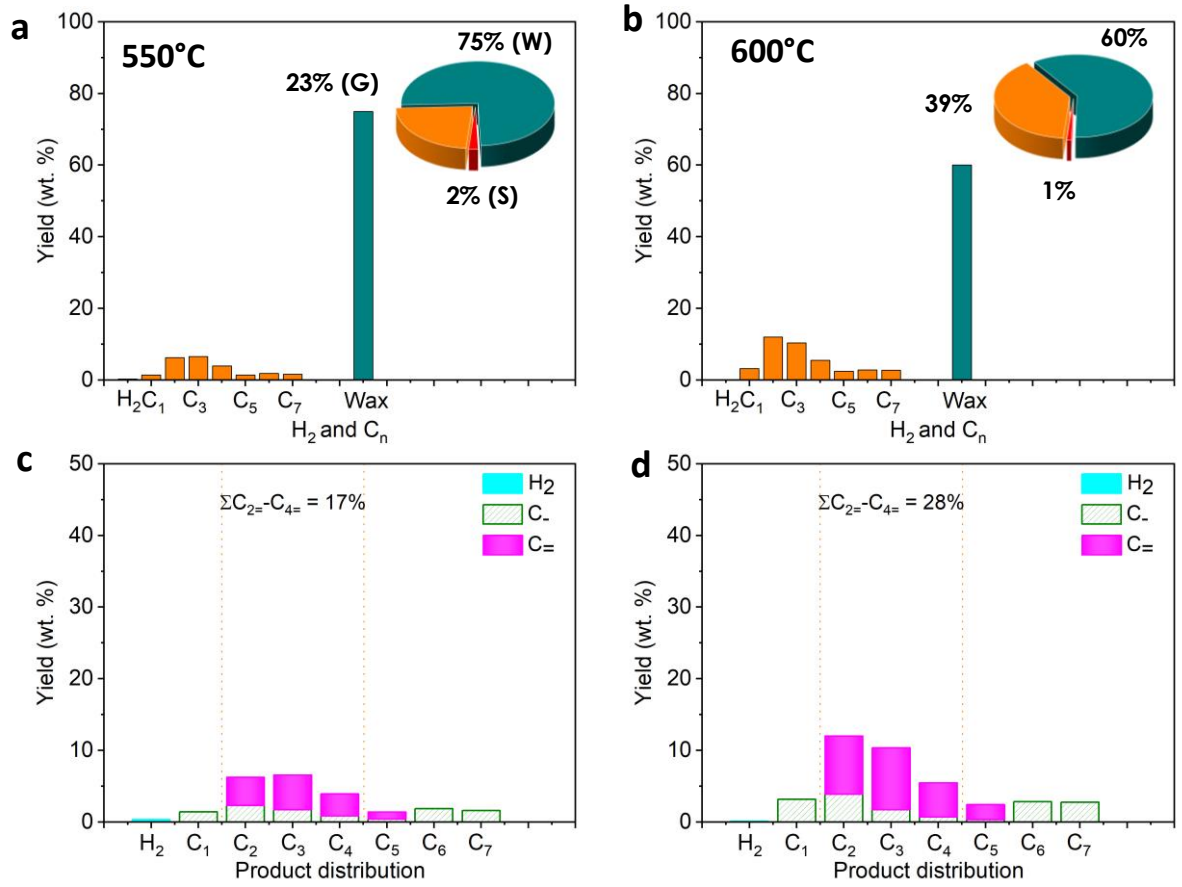

Fig. 5 | (a, b) PTO process of model HDPE on CF catalyst operated under indirect convection and conduction heating mode at different reaction temperature: 550 °C and 600 °C. The waxy fraction contains hydrocarbons ranged from C_{10} to > C_{30}. (c, d) The light olefins and aromatics hydrocarbons obtained in the different experiments. Reaction conditions: polymer weight feeding = 10 g. h^{-1} with sequential feeder, CF weight = 1.6 g (with an apparent volume of 64 cm^3), reactor diameter = 26 mm, argon flow rate = 30 mL. min^{-1}, reaction temperature = 550 °C and 600 °C, HDPE was vaporized in the first stage of the process with an electric oven set at 450 °C.

The representative SEM micrographs of the spent CF catalyst after pyrolysis experiments under IH at 500 °C are presented in Fig. 6. SEM analysis indicates the presence of a relatively thin and homogeneous carbonaceous layer, 250 nm, on the surface of the CF microfilament (Fig. 6a-c). High-resolution SEM micrograph seems to confirm that such carbonaceous layer is relatively rough with small carbon nodules ranged from 30 to 60 nm stacked from each other (Fig. 6d). In addition, as shown in Fig. 6b and c the layer of solid carbon deposit during the test is relatively homogeneous and covering well the surface of the pristine CF microfilament. According to previous results obtained on carbon-based catalysts for the catalytic methane decomposition (CMD) the deposited carbon plays directly the role of active phase for such reaction [63, 75]. Indeed, in the CMD process, as a function of the reaction no more pristine carbon surface was accessible due to the extremely high carbon deposit amount from the reaction whereas the CMD activity remains unchanged which confirms the autocatalytic characteristic of the deposited carbon to act as an active phase for the decomposition of methane. The evidence about the fact that carbon deposit could plat directly the role of catalyst for the PTO will be presented and discussed in the section dedicated to the cycling tests [63, 75]. It is also worthy to note that the carbon layer is deposited in a homogeneous way on the surface of the carbon microfilament which indicates that the entire surface of the CF participates to the process and not some very localized sites. Such layer deposition is quite surprising as generally, carbonaceous deposit is mostly performed in the form of discrete carbon nodules dispersed on the different areas of the

catalyst surface and not as thin and homogeneous one as observed in the present case. It is expected that the presence of an electrical or magnetic field could have an influence on such peculiar structure of the carbon deposit. It is worthy to note that the waste plastic pyrolysis performance remains stable, see long-term cycling tests in section 3.3, which confirms in part that the deposited carbon could also play a role of catalyst. Again, similar results have also been reported by Essyed et al. [74] during the catalytic methane decomposition process on carbon-based catalyst where the deposited carbon displays a high and stable catalytic activity, i.e. autocatalytic process. However, work is still needed to investigate such phenomenon as well as the influence of an oscillating magnetic field on the life-time or adsorption and desorption of the intermediate species as discussed in the different recent literature reports [55, 63, 74].

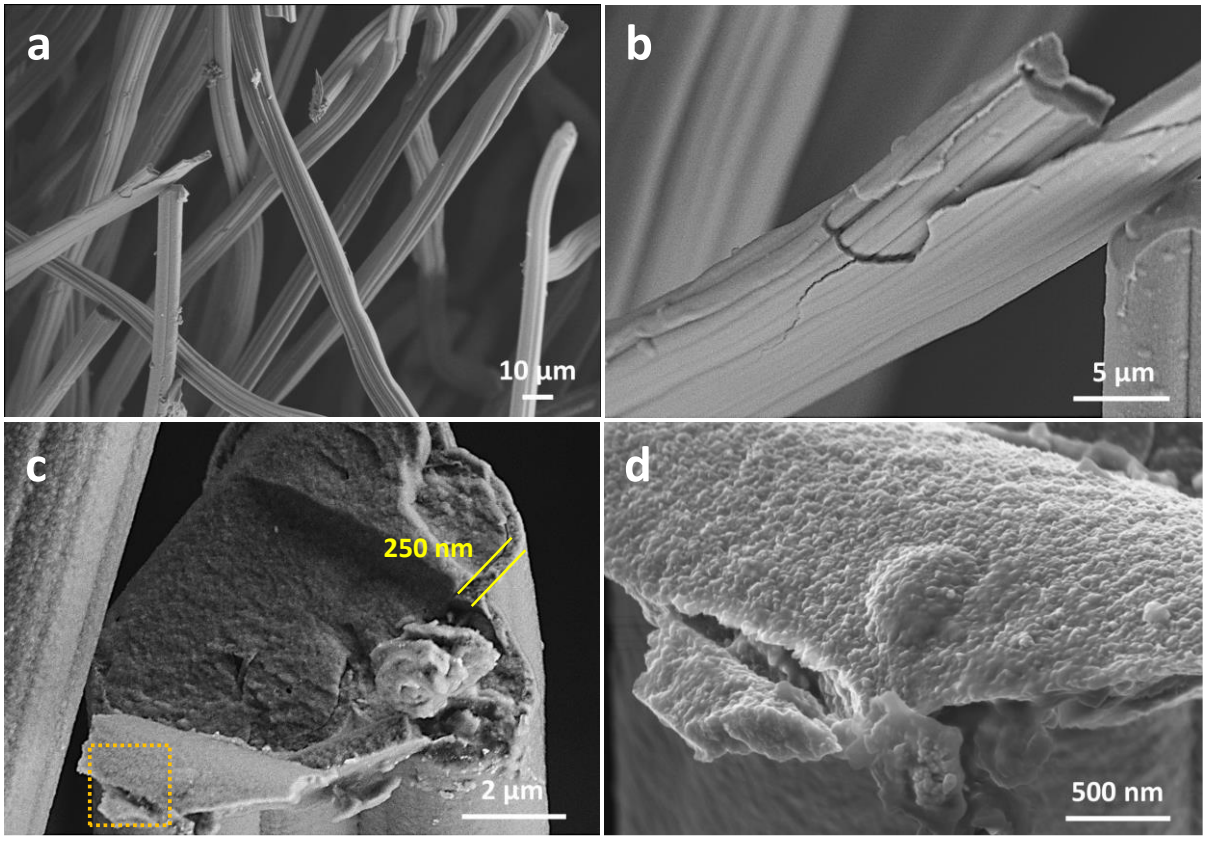

Fig. 6 | (a, b) Low magnification SEM micrographs of the spent CF catalyst after HDPE test operated under IH at 500 °C showing the presence of a carbon layer on the top surface, (c) SEM micrograph with medium resolution evidencing the homogeneous thickness of the

deposited carbon layer, (d) High-resolution SEM micrograph showing the porous structure of the carbon layer.

Raman analysis of the spent CF sample again confirms the presence of two main peaks at 1345 cm^{-1} and 1605 cm^{-1} while the I_D/I_G ratio is significantly modified with respect to the pristine sample, i.e. 0.76 vs 1.28 (Fig. 3a). The I_D/I_G ratio change could be attributed to the formation of the thin layer of carbonaceous residue on the spent catalyst with slightly higher graphitic nature, or with lower structural defects, which are mostly affecting the D peak. Another striking fact is the formation of an enlargement base around the D peak which was not observed on the pristine sample. Such widening of the D peak could also indicate that the formed carbon is consisting with long-range disordered graphite structure or to the formation of higher graphitic domain boundaries [93]. The increase of the G peak seems to indicate that crystallinity, or graphitic character, is improved on the spent CF catalyst which could be due to the well-ordered inside the individual carbon nanoparticles constituting the deposited carbon layer. The disappearance of the 2D peak could be attributed to the displacement of phonons in several stacked graphene planes which are stacked in a disordered arrangement, i.e. in-plane defects.

On the other hand, TGA spectrum also confirms a temperature shift between the fresh and spent CF samples indicating that the carbon deposit displays a slightly higher oxidative resistance, i.e. combustion peak shifted from 760 °C to 800 °C (Fig. 3b), which is in good agreement with the Raman results showing a more ordered carbon structure (Fig. 3a).

3.3 PTO with model mixed polymer

The results obtained above clearly evidence the high performance of the carbon-based materials for converting model HDPE directly to light olefins at mild reaction temperatures in a continuous mode. In order to check out if such performance could be obtained not on a model single polymer but on a representative waste polymer the same experiment was carried out using a mixture of polymers which simulates the main components of the most common sorting refusal waste: HDPE (35 wt.%), LDPE (35 wt.%), PP (20 wt.%) and PS (10 wt.%) [94, 95]. The different gas, liquid and solid residues, and the detailed products distribution obtained at different reaction temperatures are presented in Fig. 7a, c and e. At reaction temperature ≥ 480 °C the gaseous fraction remains similar at ca. 70 % of the total weight of the waste plastic converted (Fig. 7c) with a light olefins yield at around 38 % (Fig. 7d and f). At reaction temperature of 480 °C the aromatics contribute to about 10 % (Fig. 7d) while they increase to 12 % at 500 °C (Fig. 7f). It is worthy to note that at 500°C, the solid residue deposited on the CF catalyst was relatively important, compared to that obtained at lower reaction temperature, i.e. 2% at 450 °C, 6% at 480 °C and 10% at 500 °C, which could be due to the condensation reactions on the catalyst surface leading to heavier hydrocarbons and solid residue. In addition, at high reaction temperature the amount of methane also significantly increases due to extensive cracking process as depicted in Fig. 7f. NMR analysis is used again to assess the different product fractions inside the recovered liquid phase (Fig. 7g). The ^{1}H-NMR spectrum clearly evidences the presence of aromatic compounds (19 % accounting for the total carbon) inside the liquid phase similarly to that observed during the pyrolysis of model single HDPE plastic (Fig. 4e). However, by comparison with the latter, the ratios of styrene and toluene versus alkenes are slightly higher due to the presence of PS in the model mixed plastic and, terminal alkenes are little less abundant than their internal counterparts.

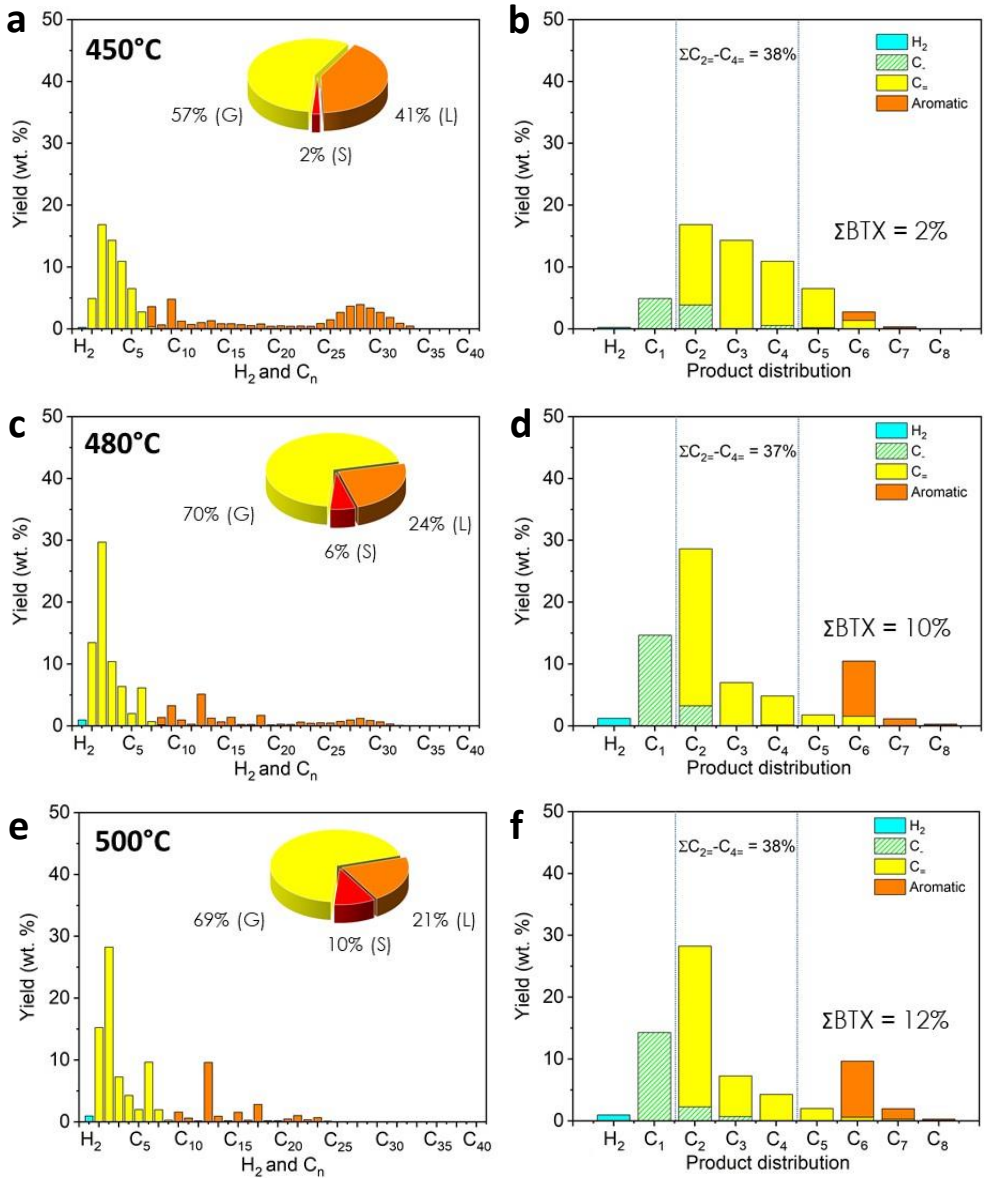
a
450°C
57% (G)
41% (L)
2% (S)
Yield (wt. %)
H2 and Cn
b
ΣC2=-C4= = 38%
H2
C.
C=
Aromatic
ΣBTX = 2%
Yield (wt. %)
Product distribution
c
480°C
70% (G)
24% (L)
6% (S)
Yield (wt. %)
H2 and Cn
d
ΣC2=-C4= = 37%
H2
C.
C=
Aromatic
ΣBTX = 10%
Yield (wt. %)
Product distribution
e
500°C
69% (G)
21% (L)
10% (S)
Yield (wt. %)
H2 and Cn
f
ΣC2=-C4= = 38%
H2
C.
C=
Aromatic
ΣBTX = 12%
Yield (wt. %)
Product distribution

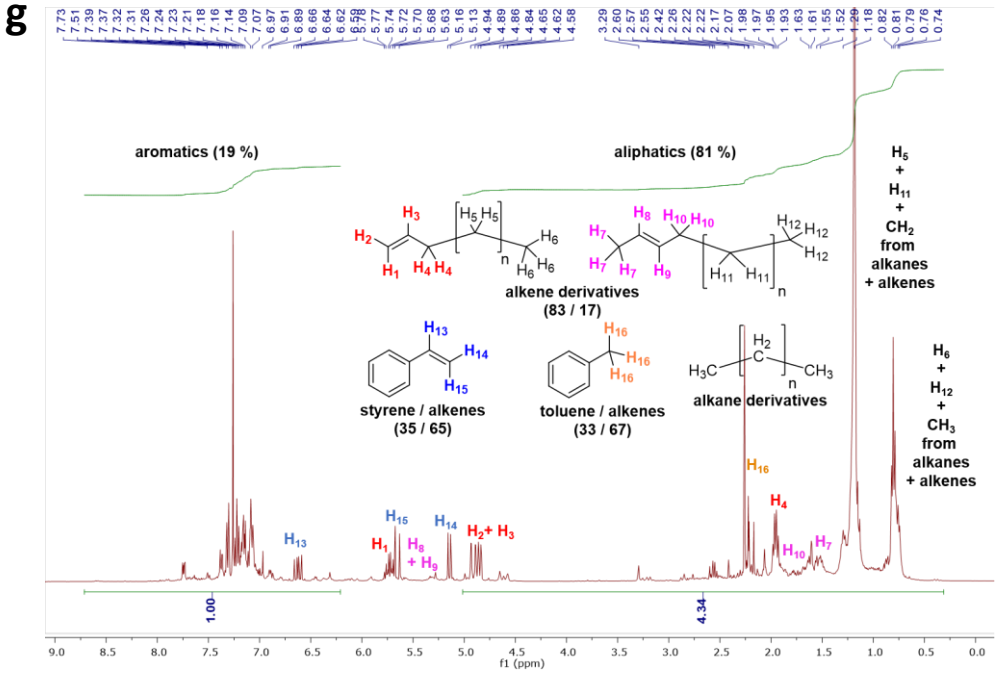

Fig. 7 | PTO process on the model mixed plastic including HPDE, PP, PS at different pyrolysis temperatures. (a, c, e) Product fraction distribution and product distribution with model mixed plastic as a function of the reaction temperature. (b, d, f) Light olefins and aromatics distribution determined in the gas-phase at different reaction temperature. (g) ^{1}H NMR of the liquid fraction obtained at 450 °C. Reaction conditions: polymer weight feeding = 10 g. h^{-1} with sequential feeder, CF weight = 1.6 g (with an apparent volume of 64 cm^{3}), reactor diameter = 26 mm, argon flow rate = 30 mL. min^{-1}, reaction temperature = 450 °C, 480 °C and 500 °C, plastic was vaporized in the first stage of the setup with an electric oven set at 450 °C and passed downward to the cracking stage operated under IH mode.

For comparison, the cracking process is also carried out on PP and PS alone and the results are presented in Fig. 8. The different gas, liquid and solid residues, and the detailed products distribution obtained at 450 °C on the two polymers are presented in Fig. 8a and b. The gaseous fraction contributes to 64 % for PP while it significantly decreases to about 16 % for PS. For PP the cracking efficiency is high and liquid fraction contributes to ca. 35 % while light olefins contribute to about 42 % and almost no aromatics (Fig. 8c). For PS the light olefins decreases in a drastic way and is accounted for about 9 % (Fig. 8d). According to these results, the cracking behavior of the model mixed polymers remains very similar to those obtain with a single polyolefins, i.e. HDPE and PP, while that of PS differs, due to the high

stability of the C-C bonds in the aromatic ring compared to the non-aromatic C-C bond and thus, the cracking of PS mostly yield styrene as product [96, 97, 98].

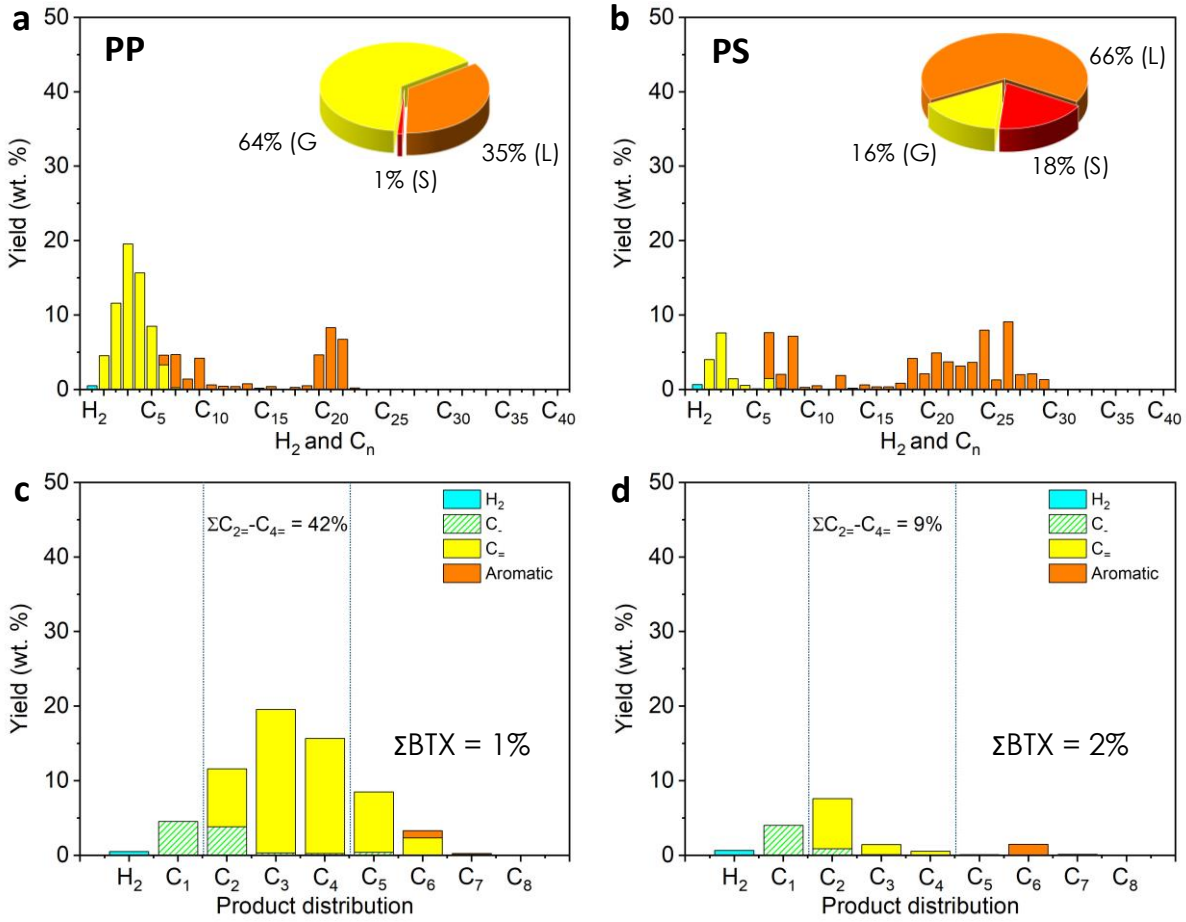

Fig. 8 | (a, b) Product fraction distribution and product distribution with PP and PS single model plastic at 450°C. (c, d) Light olefins and aromatics distribution in the gaseous stream on PP and PS feed. Reaction conditions: polymer weight feeding = 10 g. h^{-1} with sequential feeder, CF weight = 1.6 g (with an apparent volume of 64 cm^3), reactor diameter = 26 mm, argon flow rate = 30 mL. min^{-1}, reaction temperature = 450 °C, plastic was vaporized in the first stage of the setup with an electric oven set at 450 °C and passed downward to the cracking stage operated under IH mode.

The influence of the branching in the polyolefin polymers on the cracking performance is also evaluated using model HDPE and LDPE. Under the same set temperature, i.e. 450 °C, the gaseous fraction recovered from the pyrolysis of LDPE is similar compare to that obtained with HDPE, i.e. 71 % vs 70 % (Fig. 9a and b). The light olefins yield displays a

large improvement passing from 43 % for HDPE to about 49 % for LDPE (Fig. 9c and d). On the other hand, aromatics show hardly change between LDPE and HDPE charge. According to the results, LDPE displays higher light olefins production compared to HDPE which could be attributed to the multiple branching within the LDPE leading thus to a higher cracking. Such chemical recycling efficiency should be taken into account during the processing of industrial waste plastic mixture by adjusting the operated temperature in order to avoid excessive cracking.

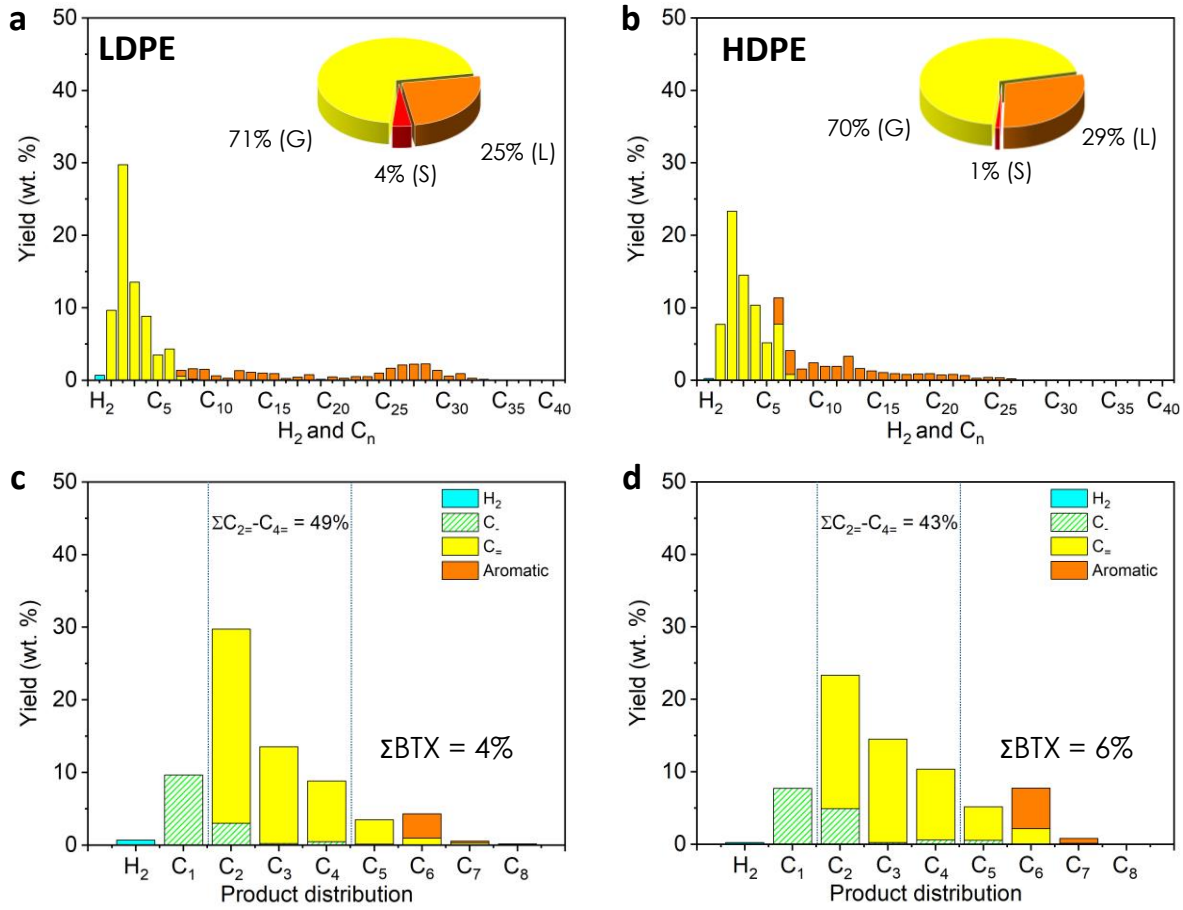

Fig. 9 | PTO process on the LDPE and HDPE model plastics at 450 °C. (a, b) Product fraction distribution and product distribution with LDPE and HDPE single model plastic at 450°C. (c, d) Light olefins and aromatics distribution in the gaseous stream on LDPE and HDPE feed. Reaction conditions: polymer weight feeding = 10 g. h^{-1} with discontinuous feeder, CF weight = 1.6 g (with an apparent volume of 6 cm^3), reactor diameter = 26 mm, argon flow rate = 30 mL. min^{-1}, reaction temperature = 450 °C, PE was vaporized in the first stage of the setup with an electric oven set at 450 °C and passed downward to the second stage operated under IH mode where cracking occurs.

3.4 PTO with industrial waste plastic mixture

According to the results obtained before, rolled CF catalyst is able to convert model HDPE plastic in one-step into light olefins (yield of ca. 43 %) and aromatics (yield of ca. 6 %). However, the results obtained could be biased as model waste plastic contains no impurities which could affect the catalyst stability. In recent report Jaydey et al. [99] have reported the hydrogenolysis of different polyethylene model waste plastic into alkanes (C_1-C_{45}) under mild conditions on ultrafine ruthenium nanoparticles. The catalyst displayed relatively high stability up to three cycles. However, the reaction carried out with commercial caps induced a reduced activity compared to the model waste plastic and was attributed to the presence of additives, in the real sample, which could influence the ruthenium activity. Such results pointed out the difficulty to perform chemical recycling with real industrial waste plastic where additives and impurities significantly harm the catalyst stability and long-term operability. Similar investigation has also been reported by Zhang et al. [100] through chloride and hydride transfer to convert polyethylene into liquid alkanes. The authors have observed that only $AlCl_3$ and $GaCl_3$ can efficiently catalyze selective deconstruction of LDPE to liquid alkanes close to ambient temperature. Again, the direct evaluation of such catalyst using industrial waste plastic is lacking of a complete assessment of its performance and stability in such process. Indeed, mixed plastics contain several impurities, additives (plasticizers and lubricants), fillers and reinforcement, and different stabilizing compounds (flame retardants, anti-oxidants and ultraviolet stabilizers) that make them difficult to reuse or recycle [101, 102]. The presence of plastic mixture, i.e. multilayer plastics, also represents a problem for the recycling, especially for mechanical recycling and chemical recycling as well due to the production of mixture products which needs to be separated post-process [103].

In order to assess the high pyrolysis performance of our system the model HDPE plastic is replaced by a real industrial mixture containing HDPE, LDPE, PS and also some

residual wood component. The PTO experiments were carried out at two reactions temperature, i.e. 450 °C and 500 °C, and the results are presented in Fig. 10. The gas, liquid and solid fraction and product distribution as a function of the reaction temperature are presented in Fig. 10 a and b. At 450 °C the gaseous fraction contributes to about 72 % while the liquid and solid fraction are 22 % and 6 %, respectively (Fig. 10a). At 500 °C the solid fraction steadily increases from 6 % to 10 % at the expense of the gaseous one (Fig. 10b). The high concentration of LDPE in the industrial waste plastic explains the production of a higher gaseous fraction due to the reactivity of the branched polymer compared to that of the HDPE as reported above. At medium temperature, i.e. 450 °C, the light olefins yield amounted to about 45 % with ethylene and propylene contributing to ca. half part and about 5 % of aromatics (Fig. 9c). At higher reaction temperature, methane becomes important while the light olefins significantly decreased, passing from 45 % to 36 % (Fig. 10c and d). It is worthy to note that some residual wooden particles are also present inside the processed waste polymer and was found trapped in the first pyrolyzed stage in the form of yellow pale powder. The process operated with such two stages pyrolysis, thus allows one to prevent the excessive fouling of the CF catalyst as the first stage acts both as pre-vaporization step and also, as scavenger guard bed for the retention of undesirable products.

^{1}H NMR spectrum of the liquid fraction recovered at the exit of the pyrolysis reactor is presented in Fig. 10e and confirms the presence of linear alkanes and alkenes, terminal derivatives being still more abundant than internal ones. By comparison, a relatively large amount of aromatics, i.e. BTX fraction contributes to about 50 % in liquid fraction, is observed but the amount of styrene and toluene derivatives remains stable and inferior with respected to alkenes. It is worthy to note that ethylene, propylene and BTX fraction are among the five most demanded chemical building blocks for petrochemical in the future, which also contribute to a high carbon footprint [57].

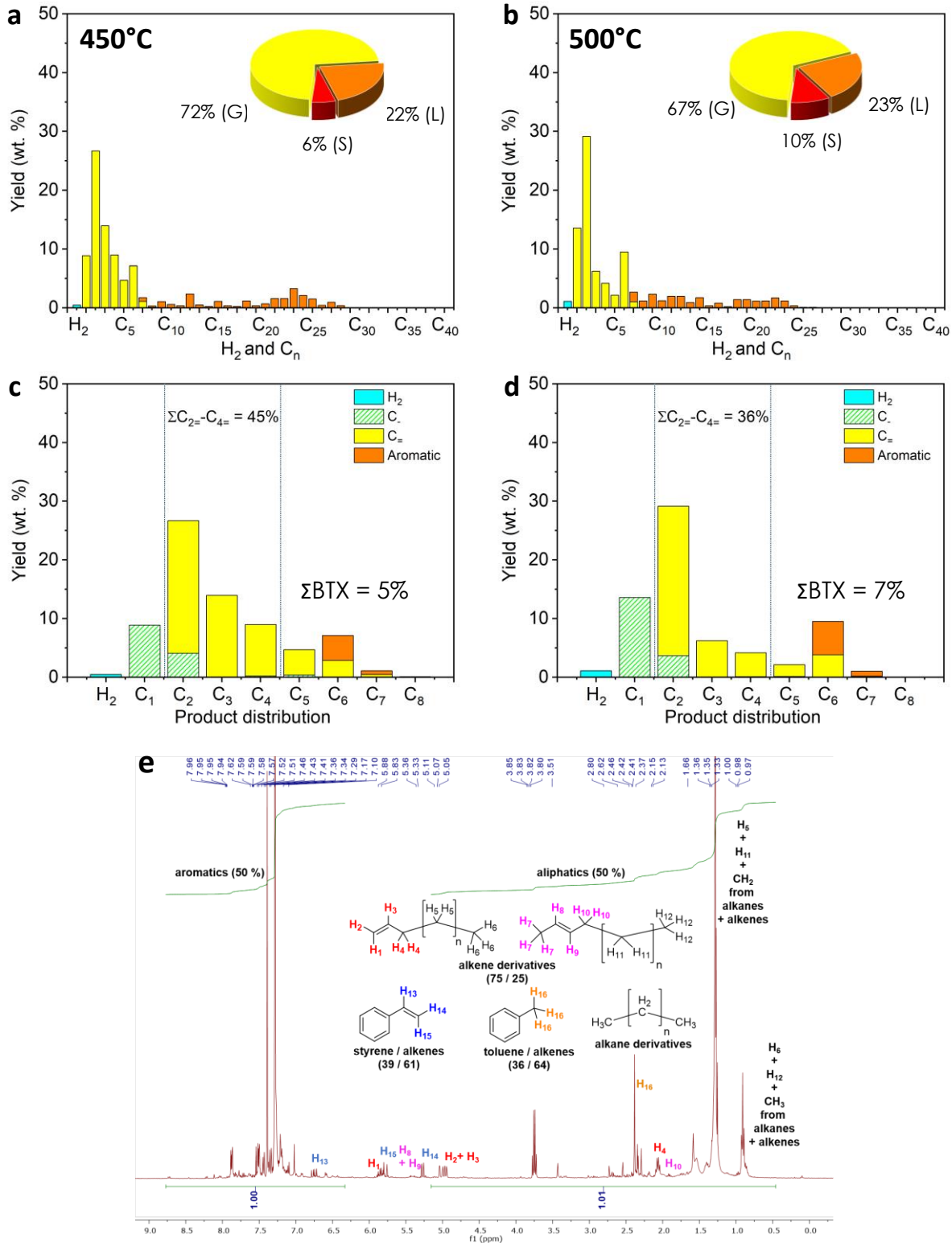

Fig. 10 | PTO process with industrial waste plastic consisting with a mixture of HDPE, LDPE, PS and residual wood on CF catalyst operated under direct IH mode. Hydrocarbon distribution and gaseous products yield at (a, c) 450 °C and (b, d) 500 °C. Reaction conditions: CF weight = 1.6 g, plastic feeding = 10 g. h^{-1}. (e) ^{1}H-NMR spectrum of the condensed liquid hydrocarbon in the exit gas stream.

3.5 Stability evaluation with industrial waste plastic

In order to assess the long-term pyrolytic performance of the CF catalyst cycling tests (6 g per test) were carried out with industrial waste plastic. The cycling tests were carried out at 450°C in order to reduce the amount of solid carbonaceous deposit according to the results obtained above. The results obtained after different number of cycles confirm the high selectivity of the rolled CF material to convert waste plastic into light olefins and the high stability of the material as no deactivation was observed between Cycle#1 and Cycle#9 (Fig. 11a to f). The liquid fraction for the different cycles was collected and displays a bright yellow color which is typical for aromatic-free hydrocarbons. The fraction distribution as a function of the cycling tests indicates that the gaseous fraction slightly decreases from 72% at the Cycle#1 to 67% for the Cycle#3 and remains stable for the following cycles (Fig. 11g) while the olefins distribution displays similar trend as a function of the cycling tests (Fig. 11h). Such results represent a significant step forward in the chemical recycling of industrial wastes as generally zeolite and metal catalysts display gradual deactivation either by surface fouling or pore plugging as a function of cycling tests [104, 105, 106, 107].

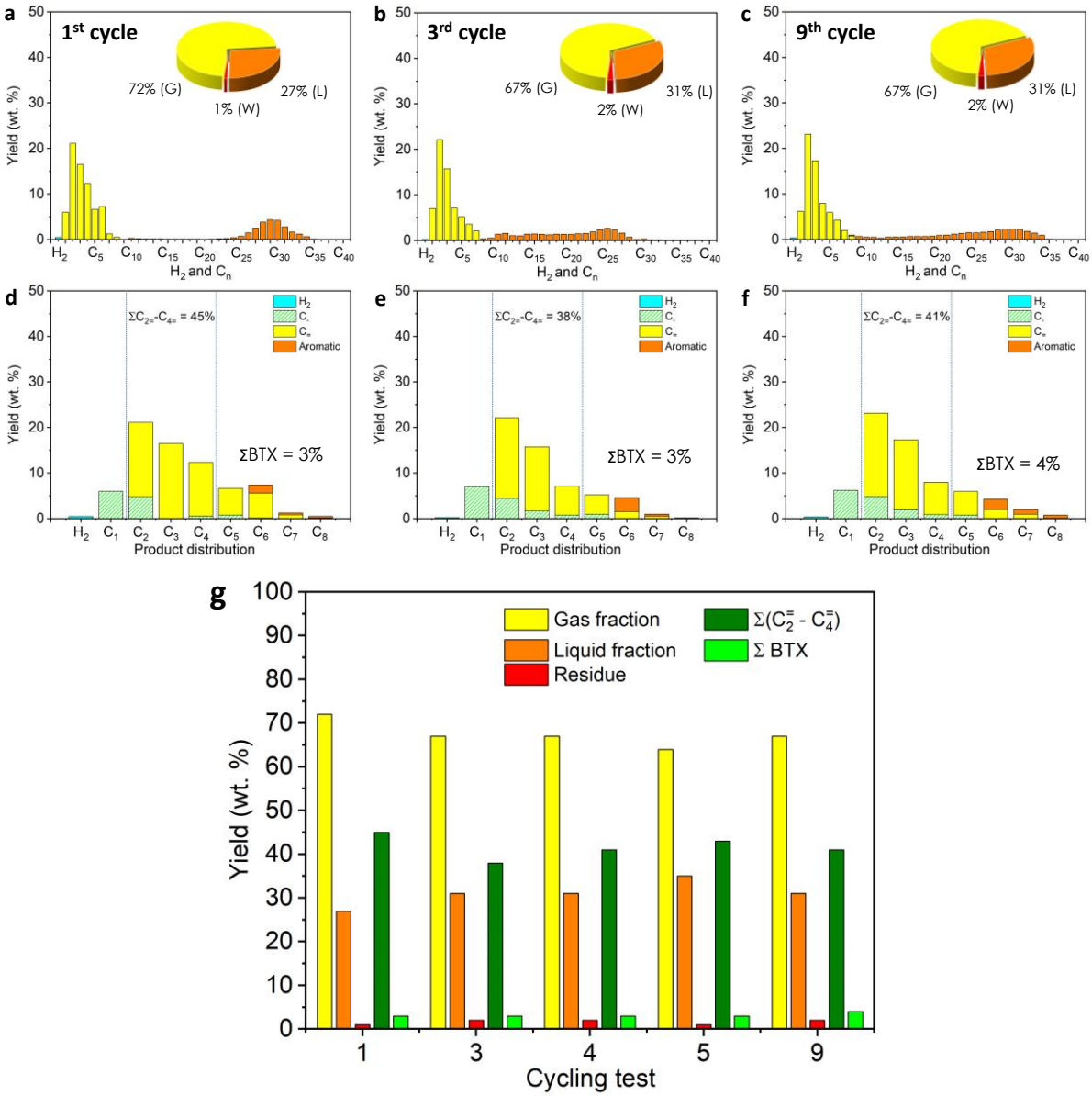

Fig. 11 | Cycling tests with industrial waste plastic on CF catalyst. Reaction conditions: pyrolysis temperature (IH) = 450 °C, rolled CF with 30 mm in height, waste plastic amount = 6 g x 9 = 54 g). For each test, the catalyst is weighted for checking the amount of carbonaceous deposit while the liquid fraction was recovered for analysis. (a to c) Fraction distribution as a function of cycling tests, (d to f) Light olefins and aromatics distribution in the gaseous fraction as a function of cycling tests, (g) Fraction and products (light olefins and aromatics) distribution in the gas phase as a function of cycling tests.

The spent CF after cycling tests was analyzed by SEM and the representative SEM micrographs are presented in Fig. 12. Low magnification SEM micrograph evidences the almost complete coverage of the pristine CF microfilaments by a thin and homogeneous layer

of carbon deposit (Fig. 12a and b). High-resolution SEM micrographs also confirm the very homogeneous and smooth surface of the carbon layer with a thickness amounted to ca. 0.5 µm (Fig. 12c and d). The deposited carbon layer displays an average thickness of ca. 0.5 µm as shown by the SEM analysis. The coated carbon layer is extremely smooth and no apparent cracks are observed. Such results could be attributed to the medium reaction temperature used in the cycling tests, i.e. 450 °C, compared to the SEM analysis of the spent CF catalyst operated at 500 °C (Fig. 6). Such coverage of the pristine CF surface by a new layer of carbon again reinforces the fact that the as-deposited carbon could play a role of catalyst for the conversion of waste plastic, either pure or mixed, into valuable products such as light olefins and aromatics.

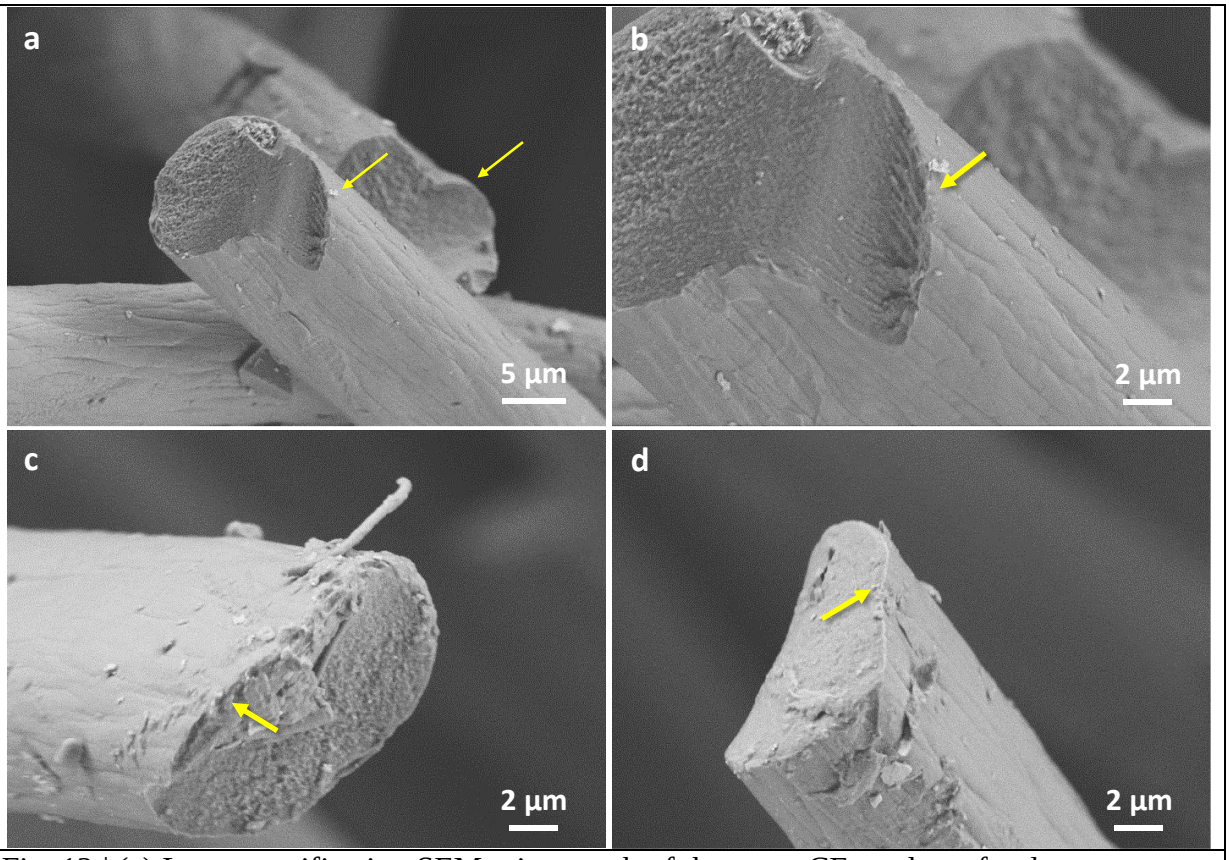

Fig. 12 | (a) Low magnification SEM micrograph of the spent CF catalyst after long-term test showing the coverage of the pristine carbon microfilament by a thin and homogeneous layer of carbon deposit. (b-d) High-resolution SEM micrographs showing the detail of the carbon deposit layer with an average thickness of ca. 0.5 µm. The carbon layer is indicated by arrows on the figure.

3.6 Influence of the contact time

The influence of the apparent contact time is also investigated for the assessment of the ability of the CF catalyst to convert waste plastic into light olefins. Increasing the CF catalyst height from 30 mm to 40 mm results in a significant improvement of the light olefins production at reaction temperature of 450 °C (Fig. 13a). At temperature of 500 °C the fraction of light olefins decreases due to the increase of the ultimate cracking leading to the formation of large amount of methane product (Fig. 13b). The results clearly evidence the important role of apparent contact time on the conversion of waste plastic, i.e. mostly polyolefins, into light olefins on CF catalyst. The results pointed out the relatively high flexibility of the process as the contact time can be varied on a large range, as well as the reaction temperature, which could allow one to cope with different waste plastic charges, and to adjust the light olefins yield without generating excessive methane as ultimate cracking product.

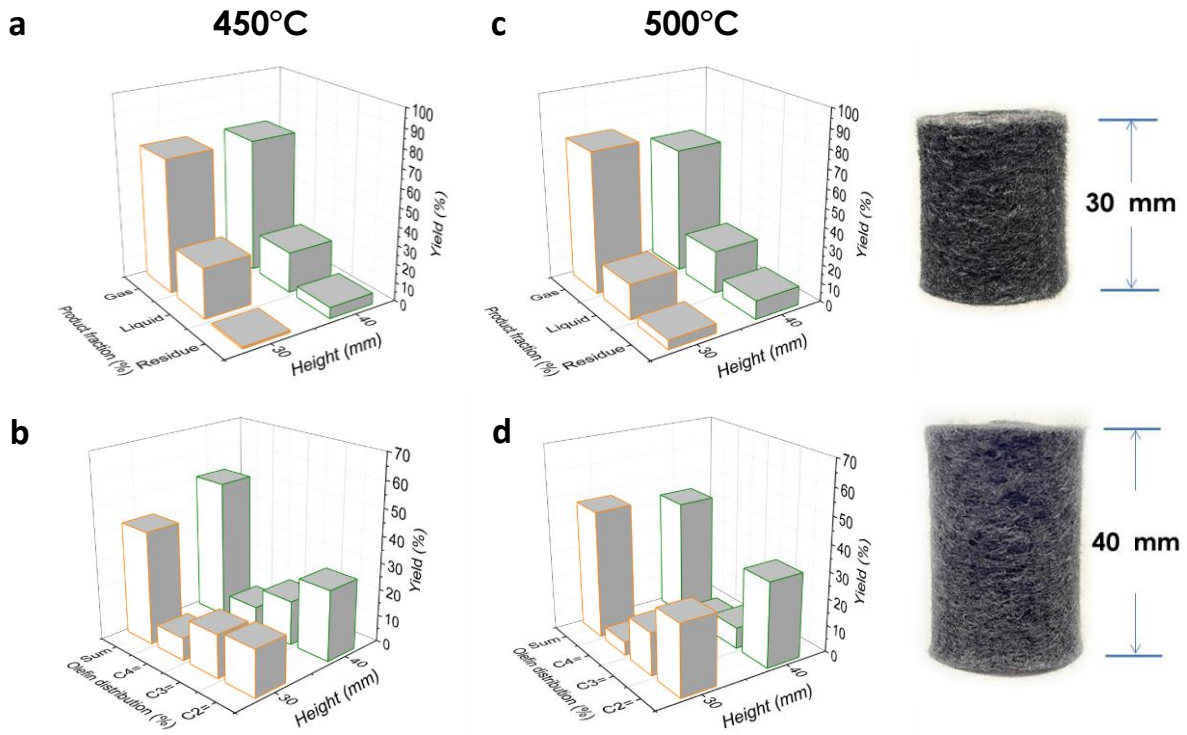

Fig. 13 | Influence of the CF catalyst length (apparent contact time) on the waste plastic pyrolysis to light olefins at different temperature. The recovered fractions and the olefins distribution are presented for different reaction temperature: (a, b) 450 °C, (c, d) 500 °C.

Digital photos of the rolled CF catalysts are presented in an inset. Reaction conditions: polymer weight feeding = 10 g. h^{-1} with discontinuous feeder, CF weight = 1.6 g (with an apparent volume of 6 cm^3), reactor diameter = 26 mm, argon flow rate = 30 mL. min^{-1}, reaction temperature = 450 °C, HDPE vaporization at the first stage with an electric oven set at 450 °C.

4. Conclusion

According to the results obtained above, one can stated that rolled CF material, displays a high selectivity towards light olefins and aromatics at mild reaction temperature, i.e. between 450 °C and 500°C, and could represent a material of choice for the development of direct and selective process for converting waste plastic (industrial mixed polymers) into valuable products using low cost metal-free carbon-based material. The reaction seems to occur by adsorption of the intermediate pyrolyzed compounds issued from the first pre-cracking stage on the surface of the CF, with exclusively geometric surface as no internal porosity is present in such material, followed by a cracking of the adsorbed long-chain hydrocarbons to yield light olefins which could be rapidly desorbed into the gas-phase. As induction heating only target heat to the solid and thus, the gas phase medium is expected to have lower temperature which could allow a rapid quenching of the desorbed light olefins and thus, reducing the secondary gas-phase reactions. The adsorbed intermediates could also reacted each other to generate aromatics. The surrounding magnetic field, even weak, could also have some influence on the radical production or reaction despite further detail investigation is still needed to get more insight about the pyrolysis mechanism.

The high yield of light olefins, especially ethylene and propylene, and aromatics on the CF materials was particularly promising as such compounds can find widespread application in numerous chemistry commodities such as feedstock for the production of polymers, oxygenates intermediates (ethylene glycol, ethylene oxide, acetone, acrylonitrile and acetaldehyde) as well as personal care products and detergents. The possibility to produce directly light olefins from waste plastic also represents an elegant way to reduce the use of

fossil fuel-based routes for the marked needs. The mixture of light olefins obtained can be easily processed at the industrial scale by various methods according to the public reports. In addition, the process also produces a substantial amount of aromatics, i.e. BTX, which represents an interesting chemical feedstock in numerous downstream processes. Another advantage relies on the use of plain carbon materials, without any additives or promoters, which display stronger resistance towards deactivation through encapsulation by deposit carbon or coke precursors, as encountered with zeolite-based materials, or chemical properties modification in the presence of organic or inorganic impurities in the industrial processed waste polymers. The carbon catalyst also displays high stability as a function of cycling tests, for both model and industrial waste plastics, which indicates that deactivation by carbon plugging is unlikely.

Acknowledgements

The authors would like to thank the SATT Conectus for financial support during the project and Mrs. A. Liegeon (SATT), Mr. N. Knepper (SATT) and R. Gresser (I2V, Innovation to Value) for helpful discussion during the project. The SEM analysis was carried out at the SEM Cronenbourg platform of the ICPEES-IPCMS (UMR 7504 CNRS) and T. Romero is gratefully acknowledged. The X-ray tomography analysis were carried out at the X-ray tomography platform of the ICS (UPR2022, CNRS) and Mr. A. Egele and D. Favier, are gratefully acknowledged for performing the analysis. The Raman analysis was carried out at the I-Cube (UMR 7357) and Mr. R. Meyer is gratefully acknowledged for the experiments and technical discussion.

Conflict of interest

The authors declare the following financial interests/personal relationships which may be considered as potential competing interests: C. D.V., L.T.P., J.M.N., C.P., H.B. and C.P.H. are inventors of patent #EP22306835.4 pending to CNRS, University of Strasbourg, BlackLeaf SAS, SICAT SAS.

CRediT authorship contribution statement

C. Duong-Viet: Methodology, Data acquisition, Experiments. **L. Truong-Phuoc:** Methodology, Data acquisition. **J.-M. Nhut:** Experimental discussion, Experiments, Formal analysis. **L. Nguyen-Dinh:** Experimental discussion, Formal analysis. **C. Michon:** Methodology, Data acquisition, Experiments, Writing. **C. Pham:** Methodology, Formal analysis, Writing. **C. Pham-Huu:** Experimental discussion, Writing, Funding, Supervision.

References

1. Geyer R., Jambeck J. R., Law K. L., Production, use, and fate of all plastics ever made, Sci. Adv. 3 (2017) e1700782.
2. Lange J.-P., Managing Plastic Waste Sorting, Recycling, Disposal, and Product Redesign, ACS Sustain. Chem. Eng. 9 (2021) 15722-15738.
3. Hussein Z. A., Shakor Z. M., Alzuhairi M.,Al-Sheikh F., Thermal and catalytic cracking of plastic waste: a review, Int. J. Environ. Anal. Chem. 103 (2023) 5920-5937.
4. Kwon J.-H., Kim J.-W., Pham T. D., Tarafdar A., Hong S., Chun S.-H., Lee S.-H., Kang D.-Y., Kim J.-Y., Kim S.-B., Jung J., Microplastics in food: a review on analytical methods and challenges, Int. J. Environ. Res. Public Health 17 (2020) 6710.
5. Barboza L. G. A., Vethaak A. D., Lavorante B. R. B. O., Lundebye A.-K., Guilhermino L., Marine microplastic debris: an emerging issue for food security, food safety and human health, Marine Poll. Bull. 133 (2018) 336-348.
6. Zhang F., Zeng M., Yappert R. D., Sun J., Lee Y.-H., LaPointe A. M., Paters B., Abu-Omar M. M., Scott S. L., Polyethylene upcycling to long-chain alkylaromatics by tandem hydrogenolysis/aromatization**,** Science 370 (2020) 437-441.
7. Liu S., Kots P. A., Vance B. C., Danielson A., Vlachos D. G., Plastic waste to fuels by hydrocracking at mild conditions, Sci. Adv. 7 (2021) eabf8283.
8. Roosen M., Mys, N., Kusenberg, M., Billen, P., Dumoulin, A., Dewulf, J., Van Geem, K. M., Ragaert, K., De Meester, S., Environ. Sci. Technol. 54 (2020) 13282-13293.
9. P.G.C. Nayanathara Thathsarani Pilapitiya , Amila Sandaruwan Ratnayake, The world of plastic waste: a review, Cleaner Mater. 11 (2024) 100220.
10. Tiwari R., Azad N., Dutta D., Yadav B. L., Kumar S., A critical review and future perspective of plastic waste recycling, Sci. Total Environ. 881 (2023) 163433.
11. Ragaert K., Delva L., Van Geem K., Mechanical and chemical recycling of solid plastic waste, Waste Management 69 (2017) 24-58.
12. Zoé O. G. Schyns Z. O. G., Shaver M. P., Mechanical Recycling of Packaging Plastics: A Review, Macromol. Rapid Commun. 42 (2021) 2000415.
13. Kumar P. S., Bharathikumar M., Prabhakaran C., Vijayan S., Ramakrishnan K., Conversion of waste plastics into low-emissive hydrocarbon fuels through catalytic depolymerization in a new laboratory scale, Int. J. Energy Environ. Eng. 8 (2017) 167.
14. Ratnasari D. K., Nahil M. A., Williams P. T., Catalytic pyrolysis of waste plastics using staged catalysis for production of gasoline range hydrocarbon oils, J. Anal. Appl. Pyrol. 124 (2017) 631.
15. Nagy A., Kuti R., The Environmental Impact of Plastic Waste Incineration, AARMS 15 (2016) 231–237.
16. Li C.-H., Zhuang H.-K., Hsieh L.-T., Lee W.-J., Tsao M.-C., PAH emission from the incineration of three plastic wastes, Environ. Inter. 27 (2001) 61- 67.
17. Schwarz, A. E., Lighart, T. N., Godoi Bizarro, D., De Wild, P., Vreugdenhil, B., van Harmelen, T., Plastic recycling in a circular economy; determining environmental performance through an LCA matrix model approach, Waste Manage. 121 (2021) 331-342.
18. Zheng, J., Suh, S., Strategies to reduce the global carbon footprint of plastics, Nat. Clim. Change **2019**, 9, 374-378.
19. Fazekas T. J., Alty J. W., Neidhart E. K., Miller A. S., Leibfarth F. A., Alexanian E. J., Diversification of aliphatic C-H bonds in small molecules and polyolefins via radical chain transfer, Science 375 (2022) 545-550.

20. Zeng M., Lee Y.-H., Strong G., LaPointe A. M., Kocen A. L., Qu Z., Coates G. W., Scott S. L., Abu-Omar M. M., Chemical Upcycling of Polyethylene to Value-Added α,ω-Divinyl-Functionalized Oligomers**,** ACS Sustainable Chem. Eng. 9 (2021) 13926-13936.
21. Meys R., Kätelhön A, Bachmann M., Winter B., Zibunas C., Suh S., Bardow A., Achieving net-zero greenhouse gas emission plastics by a circular carbon economy, Science 374 (2021) 71-76.
22. Jiao X., Zheng K., Hu Z., Zhu S., Sun Y., Xie Y., Conversion of waste plastics into value-added carbonaceous fuels under mild conditions, Adv. Mater. 33 (2021) 2005192.
23. Nakaji Y., Tamura M., Miyaoka S., Kumagai S., Tanji M., Nakagawa Y., Yoshioka T., Tomishige K., Low-temperature catalytic upgrading of waste polyolefinic plastics into liquid fuels and waxes, Appl. Catal. B 285 (2021) 119805.
24. Fakhroleslam M., Sadrameli S. M., Thermal cracking of hydrocarbons for the production of light olefins: a review on optimal process design, operation, and control, Ind. Eng. Chem. Res. 59 (2020) 12288-12303.
25. Gao Y., Neal L., Ding D., Wu W., Baroi C., Gaffney A. M., Li F., Recent advances in intensified ethylene production-a review, ACS Catal. 9 (2019) 8592-8621.
26. Monai, M., Gambino, M., Wannakao, S., Weckhuysen, B. M., Propane to olefins tandem catalysis: a selective route towards light olefins production, Chem. Soc. Rev. 50 (2021) 11503-11529.
27. Beader M., An overview of industrial processes for the production of olefins-C4 hydrocarbons, ChemBioEng Rev. 1 (2014) 136-147.
28. Zhao Z., Jiang J., Wang F., An economic analysis of twenty light olefins production pathways, J. Energy Chem. 56 (2021) 193-202.
29. Akah A., Williams J., Ghrami M., An overview of light olefins production via steam enhanced catalytic cracking, Catal. Survey Asia 23 (2019) 265-276.
30. Young B., Hawkins T. R., Chiquelin C., Sun P., Gracida-Alvarez U. R., Elgowainy A., Environmental life cycle assessment of olefins and by-products hydrogen from steam cracking of natural gas liquids, naphtha, and gas oil, J. Cleaner Prod. 359 (2022) 131884.
31. Eschenbacher, A., Varghese, R. J., Abbas-Abadi, M. S., Van Geem, K. M., Maximizing light olefins and aromatics as high value base chemicals via single step catalytic conversion of plastic waste, Chem. Eng. J. 428 (2022) 132087.
32. Onwudili, J. A., Muhammad, C., Williams, P. T., Influence of catalyst bed temperature and properties of zeolite catalysts on pyrolysis catalysis of a simulated mixed plastics sample for the production of upgraded fuels and chemicals, J. Energy Inst. 92 (2019) 1337-1347.
33. Dai L., Zhao H., Zhou N., Cobb K., Chen P., Cheng Y., Lei H., Zou R., Wang Y., Ruan R., Catalytic microwave-assisted pyrolysis of plastic waste to produce naphtha for a circular economy, Res. Conser. Recycling 198 (2023) 107154.
34. Zacharopoulou V., Lemonidou A. A., Olefins from biomass intermediates: a review, Catalysts 8 (2018) 2.
35. Seifzadeh Haghighi S., Rahimpour M. R., Raeissi S., Dehghani O., Investigation of ethylene production in naphtha thermal cracking plant in presence of steam and carbon dioxide, Chem. Eng. J. 228 (2013) 1158-1167.
36. Sadrameli S. M., Thermal/Catalytic cracking of hydrocarbons for the production of olefins: a state-of-the-art review I: thermal cracking review, Fuel 140 (2015) 102-115.
37. Mahulkar A. V., Heynderickx G. J., Marin G. B., Simulation of the coking phenomenon in the super-heated of steam cracker, Chem. Eng. Sci. 110 (2014) 31-43.

38. Barbarias I., Lopez G., Artetxe M., Arregi A., Bilbao J., Olazar M., Valorisation of different waste plastics by pyrolysis and in-line catalytic steam reforming for hydrogen production**,** Energy Convers. Manage. 156 (2018) 575-584.
39. Miandad R., Barakat M. A., Rehan M., Aburiazaiza A. S., Ismail I. M. I., Nizami A. S., Plastic waste to liquid oil through catalytic pyrolysis using natural and synthetic zeolite catalysts, Waste Management 69 (2017) 66-78.
40. Susastriawan A. A. P., Sandria A., Experimental study the influence of zeolite size on low-temperature pyrolysis of low-density polyethylene plastic waste, Therm. Sci. Eng. Prog. 17 (2020) 100497.
41. Munir D., Amer H., Aslam R., Bououdina M., Usman M. R., Composite zeolite beta catalysts for catalytic hydrocracking of plastic waste to liquid fuels, Mater. Renew. Sustain. Energy 9 (2020) 9.
42. Daligaux V., Richard R., Manero M.-H., Deactivation and regeneration of zeolite catalysts used in pyrolysis of plastic wastes-A recent and analytical review, Catalysts 11 (2021) 7770.
43. Jie X., Li W., Slocombe D., Gao Y., Banerjee I., AlMegren H., Alshihri S., Dilworth J. R., Thomas J. M., Xiao T., Edwards P. P., Microwave-initiated Catalytic Deconstruction of Plastic Waste into Hydrogen and High-Value Carbons, Nat. Catal. 3 (2020) 902-912.
44. Conk R. J., Hanna S., Shi J. X., Yang J., Ciccia N. R., Qi L., Bloomer B. J., Heuvel S., Wills T., Bell A. T., Hartwig J. F., Catalytic deconstruction of waste polyethylene with ethylene to form propylene, Science 377 (2022) 1561-1566.
45. Luo Z., Zhu X., Ma Y., Gong K., Zhu X., Alternating magnetic field initiated catalytic deconstruction of medical waste to produce hydrogen-rich gases and graphite, Cell Rep. Phys. Sci. 3 (2022) 100934.
46. Wu L., Ma H., Yan Z., Xu Q., Li Z., Improving catalyst performance of Ni-CaO-C to enhance H_2 production frombiomass steam gasification through induction heating technology, Energy Convers. Manage. 270 (2022) 1162242.
47. Wang W., Tuci G., Duong-Viet C., Liu Y., Rossin A., Luconi L., Nhut J.-M., Nguyen-Dinh L., Pham-Huu C., Giambastiani G., Induction heating: an enabling technology for theheat management in catalytic processes, ACS Catal. 9 (20199) 7921-7935.
48. Niether C., Faure S., Bordet A., Deseure J., Chatenet M., Carrey J., Chaudret B., Rouet A., Improved water electrolysis using magnetic heating of FeC–Ni core–shell nanoparticles**,** Nat. Energy 3 (2018) 476-483.
49. Nguyen H. M., Phan C. M., Liu S., Pham-Huu C., Nguyen-Dinh L., Radiofrequency induction heating powered low-temperature catalytic CO2 conversion via bi-reforming of methane, Chem. Eng. J. 430 (2022) 132934.
50. Ghosh S., Ourlin T., Fazzini P.-F., Lacroix L.-M., Tricard S., Esvan J., Cayez S., Chaudret B., Magnetically induced CO_2 methanation in continuous flow over supported nickel catalysts with improved energy efficiency, ChemSusChem 16 (2023) e202201724.
51. Almind M. R., Vendelbo S. B., Hansen M. F., Vinum M. G., Frandsen C., Mortensen P. M., Enbaek J. S., Improving performance of induction-heated steam methane reforming, Catal. Today 342 (2020) 13-20.
52. Dossow M., Klüh D., Umeki K., Gaderer M., Spliethoff H., Fendt S., Electrification of gasification-based biomass-to-X processes-a critical review and in-depth assessment, Energy Environ. Sci. 17 (2024) 925-9973.

53. Tu Z., Mu C., Yao Y., Wu L., Zou Y., Tong Z., Huang K., Recent advances in unconventional heating and external field-assisted enhancement for dry reforming of methane, Chem. Eng. J. 481 (2024) 148899.
54. Lai Truong-Phuoc L., Jean-Mario Nhut J.-M., Loïc Vidal L., Cuong Duong-Viet C., Sécou Sall S., Corinne Petit C., Christophe Sutter C., Mehdi Arab M., Alex Jourdan A., Cuong Pham-Huu C., Depleted uranium oxide supported nickel catalyst for autothermal CO_2 methanation in non-adiabatic reactor under induction heating, J. Energy Chem. 85 (2023) 310-323.
55. Wang C., Su S., Li Q., Lv X., Xu Z., Chen J., Jia H., Monolithic catalyst of Ni foam supported MnOx for boosting magnetocaloric oxidation of toluene, Environ. Sci. Technol. 58 (2024) 1410-1419.
56. Pisciotta M., Pilongé H., Feldmann J., Jacobson R., Davids J., wett S., Sasso Z., Wilcox J., Current state of industrial heating and opportunities for decarbonization, Proc. Energy Combust. Sci. 91 (2022) 100982.
57. Schiffer, Z. J., Manthiram, K. Electrification and Decarbonization of the Chemical Industry. *Joule* 1 (2017) 10-14.
58. Barton J.L., Electrification of the chemical industry, Science 368 (2020) 1181-1182.
59. Mallapragada D. S., Dvorkin Y., Modestino M. A., Esposito D. V., Smith W. A., et al., Decarbonization of the chemical industry through electrification: barriers and opportunities, Joule 7 (2023) 23-41.
60. Thiel G. P., Stark A.K., To decarbonize industry, we must decarbonize heat, Joule 5 (2021) 531-550.
61. Wang W., Duong-Viet C., Tuci G., Liu Y., Rossin A., Luconi L., Nhut J.-M., Nguyen-Dinh L., Giambastiani G., Pham-Huu C., Highly nickel-loaded g-alumina composites for a radiofrequency-heated, low-temperature CO_2 methanation scheme, ChemSusChem 13 (2020) 5468-5479.
62. Yan Y., Li N., Pan Y., Shi L., Xie G., Liu Z., Liu Q., Hydrogen-rich syngas production from tobacco stem pyrolysis in an electromagnetic induction heating fluidized-bed reactor, Int. J. Hydrogen Energy 68 (2024) 1271-1280.
63. Essyed A., Pham X.-H., Truong-Phuoc L., Romero T., Nhut J.-M., Vidal L., Brazier A., Dath J.-P., Dumont M., Pham-Huu C., High-efficiency graphene-coated macroscopic composite for catalytic methane decomposition operated with induction heating, Chem. Eng. J. 485 (2024) 150006.
64. Francke L., Benquet C., Dath J.-P., Truong-Phuoc L., Nhut J.-M., Pham-Huu C., Process for the production of hydrogen and carbon by catalytic non-oxidative decomposition of hydrocarbons, EU Pat. Appl. No. EP21306495.9 deposited on October 27, 2021, assigned to TotalEnergies SE, University of Strasbourg and CNRS.
65. Duong-Viet, C., Pham, C., Pham-Huu, C., Truong-Phuoc, L., Nhut, J.-M., Ba, H., Lafue, Y., Wambergue, S., Eur. Pat. Appl. No. EP, filed on August 24, 2022, assigned to the CNRS, University of Strasbourg, BlackLeaf SAS, and Sicat SAS, 2022.
66. Xu Z., Duong-Viet C., Ba H., Li B., Truong-Huu T., Nguyen-Dinh L., Pham-Huu C., Gaseous Nitric Acid Activated Graphite Felts as Hierarchical Metal-Free Catalyst for Selective Oxidation of H_2S, Catalysts 8 (2018) 145.
67. Oswald S., Havel M., Gogotsi Y., Monitoring oxidation of multiwalled carbon nanotubes by Raman spectroscopy, J. Raman Spectro. 38 (2007) 728-736.
68. Gholami Z., Gholami F., Tisler Z., Vakili M., A review on the production of light olefins using steam cracking of hydrocarbons, Energies 14 (2021) 8190.

69. Karaba A., Dvorakova V., Patera J., Zamostny P., Improving the steam-cracking efficiency of naphtha feedstocks by mixed/separate processing, J. Anal. Appl. Pyrolysis 146 (2020) 104768.
70. Lopez A., de Marco I., Caballero B. M., Laresgoiti M. F., Adrados A., Influence of time and temperature on pyrolysis of plastic wastes in a semi-batch reactor**,** Chem. Eng. J. 173 (2011) 62-71.
71. Lopez A., de Marco I., Caballero B. M., Laresgoiti M. F., Adrados A., Aranzabal A., Catalytic pyrolysis of plastic wastes with two different types of catalysts: ZSM-5 zeolite and Red Mud, Appl. Catal. B 104 (2011) 211-219.
72. Mastral J. F., Berrueco C., Gea M., Ceamanos J., Polym. Degrad. Stab. 91 (2011) 3330.
73. Ramirez A., Hueso J. L., Mallada R., Santamaria J., In situ temperature measurements in microwave-heated gas-solid catalytic systems. Detection of hot spots and solid-fluid temperature gradients in the ethylene epoxidation reaction, Chem. Eng. J. 316 (2017) 50-60.
74. Stefanidis G. D., Munoz A. N., Sturn G. S. J., Stankiewicz A., A helicopter view of microwave application to chemical processes: reactions, seperations, and equipment concepts, Rev. Chem. Eng. 30 (2014) 233-259.
75. Essyed A., PhamX.-H., Truong-Phuoc L., Romero T., Dath J.-P., Nhut J.-M., Brazier A., Vidal L., Nguyen-Dinh L., Pham-Huu C., Catalytic methane decomposition process on carbon-based catalyst under contactless induction heating, Chem. Synth. (2024).
76. Julian I., Ramirez H., Hueso J. L., Mallada R., Santamaria J., Non-oxidative methane conversion in microwave-assisted structured reactors, Chem. Eng. J. 377 (2019) 119764.
77. Bursavich J., Abu-Laban M., Muley P. D., Boldor D. Hayes D. J., Thermal performance and surface analysis of steel-supported platinum nanoparticles designed for bio-oil catalytic upconversion during radio frequency-based inductive heating, Energy Conv. Management 183 (2019) 689-697.
78. Pinol R., Brites C. D. S., Bustamante R., Martinez A., Silva N. J. O., Munillo J. L., Cases R., Carrey J., Estepa C., Sosa C., et al., Joining time-resolved thermometry and magnetic-induced heating in a single nanoparticle unveils intriguing thermal properties, ACS Nano 9 (2015) 3134-3142.
79. Neither C., Faure S., Borded A., Deseure J., Chatenet M., Carrey J., Chaudret B., Rouet A., Improved water electrolysis using magnetic heating of FeC-Ni core-shell nanoparticles, Nat. Energy 3 (2018) 476-483.
80. Zhou G., Wang P., Li H., Hu B., Sun Y., Huang R., Liu L., Spin-state reconfiguration induced by alternating magnetic field for efficient oxygen evolution reaction, Nat. Commun. 12 (2021) 4827.
81. Ren Y., Liao Z., Yang Y., Sun J., Jiang B., Wang J., Yang Y., Direct prediction of steam cracking products from naphtha bulk properties: application of the two sub-networks ANN, Front. Chem. Eng. 4 (2022) 983035.
82. Y. Zhang, D. Duan, H. Lei, E. Villota, R. Ruan, Jet fuel production from waste plastics via catalytic pyrolysis with activated carbons, Appl. Energy 251 (2019) 113337.
83. Duong-Viet C., Truong-Phuoc L., Nguyen-Dinh L., Michon C., Nhut J.-M., Pham C., Ba H., Pham-Huu C., Magnetic induction assisted pyrolysis of plastic waste to liquid hydrocarbons on carbon catalyst, Mater. Today Catal. 3 (2023) 100028.
84. Kiatphuengporn S., Jantaratana P., Limtrakul J., Chaneonpanich M., Magnetic field-enhanced catalytic CO_2 hydrogenation and selective conversion to light hydrocarbons over Fe/MCM-41 catalysts, Chem. Eng. J. 306 (2016) 866-875.

85. Liu D., Huang Y., Hu J., Wang B., Lu Y., Multiscale catalysts under magnetic fields: methodologies, advances and trends, ChemCatChem 14 (2022) e202200889.
86. Harmon N. J., Flatté M. E., Distinguishing spin relaxation mechanism in organic semiconductors, Phys. Rev. Lett. 110 (2013) 176602.
87. Ikeya N., Woodward J. R., Cellular autofluorescence is magnetic field sensitive, PNAS 118 (2021) e2018043118.
88. Rodgers C. T., Magnetic field effects in chemical systems, Pure Appl. Chem. 81 (2009) 19-43.
89. Coey M., Sanvito S., The magnetism of carbon, Phys. World 17 (2004) 33-37.
90. Gao Y., Feng X., Gong B.-C., Zhong C., Yang S. A., Liu K., Lu Z.-Y., Theoretical design of all-carbon networks with intrinsic magnetism, Carbon 1177 (2021) 11-18.
91. Esquinazi P., Höhne R., Magnetism in carbon structures, J. Magn. Magn. Mater. 290-291 (2005) 20-27.
92. Adogwa A., Chukwu E., Malaj A., Punyapu V. R., Chamness O., Glisson N., Bruce B., Lee S., Zachman M. J., Bruce D. A., Getman R. B., Mefford O. T., Yang M., Catalytic reaction triggered by magnetic induction heating mechanistically distinguishes itself from the standard thermal reaction, ACS Catal.14 (2024) 4008-4017.
93. Chuang C. C., Liu W.-L., Chen W.-J., Huang J.-H., Temperature and substrate dependence of structure and growth mechanism of carbon nanofiber, Appl. Surf. Sci. 254 (2008) 4681-4687.
94. Karthick K., Mohan Ramana V., Muralikrishnan M. S., Vishnuvardhan N., Naveen Kumar S., Effects of various reinforcement on mechanical properties of plastic block: A review, Journal of Physics: Conference Series 2054 (2021) 012075.
95. Pavel A., Kots P. A., Brandon C. Vance B. C., Caitlin M. Quinn C. M., Cong Wang C., Dionisios G. Vlachos D.G., A two-stage strategy for upcycling chlorine-contaminated plastic waste, Nat. Sustain. 6 (2023) 1258–1267.
96. Maafa I. M., Pyrolysis of polystyrene waste: a review, Polymers 13 (2021) 2225.
97. Liu Y., Qian J., Wang J., Pyrolysis of polystyrene waste in a fluidized-bed reactor to obtain styrene monomer and gasoline fraction, Fuel Proc. Technol. 62 (2000) 45-55.
98. Hassibi N., Vega-Bustos Y. A., Aissaoui M. H., Mauviel G., Burklé-Vitzthum V., Thermochemical recycling of polystyrene by pyrolysis: importance of the reflux to maximize the production of styrene and BTEX, Ind. Eng. Chem. Res. 62 (2023) 133432-13439.
99. Jayden S. D., Martin A. J., Usteri M.-E., Chikri K., Eliasson H., Erni R., Pérez-Ramirez J., Consumer grade polyethylene recycling via hydrogenolysis on ultrafine supported rhuthenium nanoparticles, Angew. Chem. Int. Ed. 63 (2024) e202317526.
100. Zhang W., Yao H., Khare R., Zhang P., Yang B., Hu W., Ray D., Hu J., Camaioni D. M., Wang H., Kim S., Lee M.-S., Sarazen M. L., Chen J. G., Lercher J. A., Chloride and hydride transfer as keys to catalytic upcycling of polyethylene into liquid alkanes, Angew. Chem. Int. Ed. 136 (2024) e202319580.
101. Zweifel H., Maier R. D., Schiller M., Plastics additives handbook 6th edn, Hanser Publications (2009).
102. Hahladakis, J. N., Velis, C. A., Weber, R., Iacovidou, E., Purnell, P. An overview of chemical additives present in plastics: migration, release, fate and environmental impact during their use, disposal and recycling. J. Hazard. Mater. 344 (2018) 179–199.
103. Mirkarimi, S. M. R., Bensaid, S., Chiaramonti, D. Conversion of mixed waste plastic into fuel for diesel engines through pyrolysis process: a review. Appl. Energy 327 (2020) 120040.

104. Zhou N., Dai L., Lyu Y., Wang Y., Li H., Cobb K., Chen P., Lei H., Ruan R., A structured catalyst of ZSM-5/SiC foam for chemical recycling of waste plastics via catalytic pyrolysis, Chem. Eng. J. 440 (2022) 135836.
105. Lopez A., de Marco I., Caballero B. M., Adrados A., Laresgoiti M. F., Deactivation and regeneration of ZSM-5 zeolite in catalytic pyrolysis of plastic wastes, Waste Management 31 (2011) 1852-1858.
106. Barbarias I., Lopez G., Amutio M., Artetxe M., Alvarez J., Arregi A., Bilbao J., Olazar M., Steam reforming of plastic pyrolysis model hydrocarbons and catalyst deactivation, Appl. Catal.: Gen. 527 (2016) 152-160.
107. Ochoa A., Bilbao J., Gayubo A. G., Castano P., Coke formation and deactivation during catalytic reforming of biomass and waste pyrolysis products: a review, Renew. Sustain. Energy Rev. 119 (2020) 109600.